

This discussion paper is/has been under review for the journal Atmospheric Chemistry and Physics (ACP). Please refer to the corresponding final paper in ACP if available.

Developing and bounding ice particle mass- and area-dimension expressions for use in atmospheric models and remote sensing

E. Erfani^{1,2} and D. L. Mitchell¹

¹Desert Research Institute, Reno, Nevada, USA

²Graduate Program in Atmospheric Sciences, University of Nevada, Reno, Nevada, USA

Received: 21 September 2015 – Accepted: 7 October 2015 – Published: 22 October 2015

Correspondence to: E. Erfani (ehsan@nevada.unr.edu)

Published by Copernicus Publications on behalf of the European Geosciences Union.

Ice particle mass- and area-dimension expressions

E. Erfani and
D. L. Mitchell

Title Page

Abstract

Introduction

Conclusions

References

Tables

Figures



Back

Close

Full Screen / Esc

Printer-friendly Version

Interactive Discussion



Ice particle mass- and area-dimension expressions

E. Erfani and
D. L. Mitchell

Title Page

Abstract

Introduction

Conclusions

References

Tables

Figures

◀

▶

◀

▶

Back

Close

Full Screen / Esc

Printer-friendly Version

Interactive Discussion



this temperature range. We further postulate that ice particle mass estimates at colder temperatures, based on 2D-S probe ice particle projected area measurements, should be reasonable provided that the ice particle shape composition of the PSD does not significantly change at these colder temperatures. Moreover, we assume that a similar shape composition for anvil cirrus for a given temperature range relative to the shape composition in synoptic cirrus from -40 to -20 °C justifies using the 2D-S probe mass estimates (based on area measurements) for these anvil cirrus. As a proxy for ice particle shape, we use the mean area ratio (AR) for a given ice particle size-bin, where the AR is the measured particle area divided by area of the circle defined by the particle's maximum dimension. This assumption extends this m - D parameterization down to -55 °C. More details about this approach will now be given.

SCPP (see Sect. 2.2) provides unique direct measurements of mass for ice particles, with many SCPP ice particles having ice particle shapes similar to those found in cirrus clouds. Therefore, we used this data subset for size greater than $100\ \mu\text{m}$ and CPI data (see Sect. 2.4) for size less than $100\ \mu\text{m}$. Only those SCPP ice particles having formation temperatures between -20 and -40 °C (based on observed habits) were selected. For other temperature ranges of synoptic clouds and for all temperature ranges of anvil clouds, estimated 2D-S (see Sect. 2.3) mass is used for size greater than $200\ \mu\text{m}$ and estimated CPI mass for size less than $100\ \mu\text{m}$. Since direct measurement of projected area is available for both 2D-S and CPI data, 2D-S area is used for size greater than $200\ \mu\text{m}$ and CPI area is used for size less than $200\ \mu\text{m}$ for all temperature ranges. Additional details are given below.

2.2 SCPP measurements

SCPP was a 3 year field study funded by the Bureau of Reclamation where the shapes, maximum dimensions and masses of 4869 ice particles were determined. While greater magnification was used to photograph the ice particles during the last year, for purposes of measuring ice particle size and mass, the lower magnification ($25\times$) was sufficient. In this study, we consider those ice particles measured during

Ice particle mass- and area-dimension expressions

E. Erfani and
D. L. Mitchell

[Title Page](#)[Abstract](#)[Introduction](#)[Conclusions](#)[References](#)[Tables](#)[Figures](#)[Back](#)[Close](#)[Full Screen / Esc](#)[Printer-friendly Version](#)[Interactive Discussion](#)

the SCPP that have shapes initially formed between -20 and -40°C . Moreover, the objective of M1990 was to develop m - D power laws for specific ice particle habits or shape categories (e.g. rimed column aggregates), whereas the objective of this study is to develop m - D and A - D expressions that are representative of all ice particles for a given cloud type and temperature interval, suitable for use in climate models.

Such field observations, conducted during winter storms in the Sierra Nevada Mountains, provided measurements for each individual ice particle sampled, including date and time, maximum dimension, mass, shape (if identifiable), crude level of riming (light, moderate, heavily rimed, or graupel), and temperature range that produces the observed ice particle shape. Software was created to extract any combination of ice particle shapes. For the winter storms sampled, most of the cold habit ice crystals are expected to originate between -20 and -40°C , although cloud tops colder than -40°C are possible. Ice particle shapes associated with $T < -20^{\circ}\text{C}$ that were measured during this field study include short columns (aspect ratios were < 2) and combinations thereof, side planes and their aggregates, bullets, bullet rosettes and aggregates thereof, and combinations of any of these crystal types.

2.3 2D-S probe

PSDs were sampled using the 2D-S probe, which measures the size-resolved concentrations of ice particle number and projected area. A total of 193 synoptic ice cloud PSDs and 115 anvil cirrus PSDs were sampled and analyzed. Ice particle concentrations were measured down to $10\ \mu\text{m}$ (5 – $15\ \mu\text{m}$ size bin) and up to $1280\ \mu\text{m}$ in ice particle length. Ice particle mass is not directly measured, but is estimated using a power law that relates ice particle projected area to mass (Baker and Lawson, 2006; hereafter BL2006). This relationship was developed from a subset of ice particles (865 particles) measured during SCPP. Using image analysis software, the projected area of ice particles in this subset was calculated from their photographed magnified images. The BL2006 study found that ice particle projected area was a more reliable predictor of particle mass than was maximum dimension. Their m - A power law was derived from

Ice particle mass- and area-dimension expressions

E. Erfani and
D. L. Mitchell

Title Page

Abstract

Introduction

Conclusions

References

Tables

Figures

◀

▶

◀

▶

Back

Close

Full Screen / Esc

Printer-friendly Version

Interactive Discussion

many types of ice particle habits or shapes, and of the 550 identifiable ice particles, 36% were moderately or heavily rimed. This m - A power law is now commonly used to estimate size-resolved mass concentrations from 2D-S probe measurements of projected area. Integrating these mass concentrations over the PSD, the PSD IWC is determined.

IWCs determined in this way have been compared to IWCs directly measured by the Counterflow Virtual Impactor (CVI) probe during the Tropical Composition, Cloud and Climate Coupling (TC4) field campaign (Lawson et al., 2010), where the 2D-S and CVI probes were co-located on the same aircraft with identical sampling times. A regression line relating the 2D-S and CVI IWC measurements had a coefficient of determination (R^2) of 0.88, with 2D-S IWCs being 82% of CVI IWCs on average.

The methodology for extracting m - D expressions from 2D-S probe data was first described in Mitchell et al. (2010), and is briefly described here. The mean ice particle mass is calculated for each size-bin of the 2D-S probe by dividing the mass concentration in the bin by the measured number concentration (N) in the bin. In this way the mean bin mass is related to bin midpoint size for each size-bin of the 2D-S probe. The relationship between m and D can then be characterized by plotting mean bin mass against bin midpoint size and fitting the data to an equation of m and D . This was done for the SPARTICUS 2D-S data as described below.

The processing of the 2D-S probe SPARTICUS data is described in Mishra et al. (2014). The original 2D-S data used in this study had been processed using the M1 technique for measuring ice particle length and area (see Appendix A in Lawson, 2011). However, the M1 method does not insure that the ice particle is completely imaged within the sample volume (i.e. that no portion is beyond the photodiode array), and it uses the length parameter along the direction of travel (L_1 ; see Appendix A) for maximum dimension. To overcome these drawbacks, the 2D-S data used here were processed using the newly developed M7 method that insures that the ice particles are completely imaged within the sample volume (“all-in” criteria), and this method uses the most accurate estimate for maximum dimension. The 2D-S data were then further

processed to insure that ice particle mass and projected area did not exceed that of an ice sphere having a diameter equal to the ice particle maximum dimension.

PSDs for each cloud type (synoptic or anvil) were partitioned into temperature intervals of 5 °C and the PSDs within each temperature interval were averaged to produce 9 mean PSDs (one for each T -interval) for synoptic and 9 mean PSDs for anvil ice clouds. This covered a temperature range of -20 to -65 °C for both synoptic and anvil ice clouds.

While ice clouds at temperatures warmer than -38 °C might be mixed phase (containing both liquid water and ice), all PSDs were examined for the presence of liquid water using a combination of Forward Scattering Spectrometer Probe (FSSP), CPI and 2D-S probes and relative humidity measurements using the Diode Laser Hygrometer (DLH) probe. Only PSDs not associated with evidence of liquid water were used in this analysis as described in Mishra et al. (2014). Moreover, the PSD selection process identified cloud regions where cloud extinction and median mass size were relatively stable (relatively invariant with time), making it unlikely that liquid water was present. On the other hand, it is possible that some ice particles sampled were rimed if riming occurred at levels above the level being sampled (considered unlikely for these temperatures). The number of PSDs found in each temperature interval is shown for synoptic and anvil ice clouds in Fig. 2.

There is an out-of-focus problem affecting the 2D-S measurements of projected area, specifically for ice particle sizes less than 200 μm . For this size range, many images are out-of-focus with artificial holes in the middle, so that particles have an appearance similar to doughnuts, and the projected area of these images is overestimated (Korolev, 2007). Therefore, we used the 2D-S M7 projected area for ice particle sizes larger than 200 μm , and the CPI projected area for sizes smaller than 200 μm (see next subsection).

Ice particle mass- and area-dimension expressions

E. Erfani and
D. L. Mitchell

Title Page

Abstract

Introduction

Conclusions

References

Tables

Figures



Back

Close

Full Screen / Esc

Printer-friendly Version

Interactive Discussion



2.4 CPI probe

The CPI probe provides digital images of particles that pass through the sample volume at speeds up to 200 ms^{-1} . The images were processed via CPIview software to determine ice particle length, width, projected area, perimeter, and crystal habits, with the resolution of $2.3 \mu\text{m}$, and for particles in the size range of $10\text{--}2000 \mu\text{m}$ (Lawson et al., 2001). The majority of the CPI images are in-focus, and a few of them that are out-of-focus are resized smaller using Korolev focus correction (Korolev et al., 1998). For this reason, CPI projected area is more reliable compared to the 2D-S for ice particle size less than $200 \mu\text{m}$ and we used CPI projected area for sizes less than $200 \mu\text{m}$.

A discontinuity in projected area is observed between the 2D-S using M1 processing and the CPI for $D \approx 200 \mu\text{m}$, with 2D-S area being larger than CPI area by a factor of 1.54 ± 0.18 . There are three factors that contribute to this discrepancy; first, 2D-S M1 for larger sizes can still be out-of-focus, though less than that for smaller sizes; second, it seems that 2D-S overestimates size with errors being $10\text{--}30\%$, even when they are in-focus; third, there are inherent differences between CPI and 2D-S, since they are two different instruments that use two different measurement techniques. Using the M7 data processing, the 2D-S area is larger than CPI area by a factor of 1.30 ± 0.15 , showing that M7 and CPI are more self-consistent than M1 and CPI. The number of ice particles imaged by the CPI that were used in this study is 224 719. Hence, the CPI sampling statistics in each size bin is quite good.

The CPI probe does not measure ice particle mass and BL2006 *m-A* method is not justified for sizes smaller than $150 \mu\text{m}$, because it was derived from SCPP data with ice particles having sizes generally greater than $150 \mu\text{m}$. Therefore, we suggest a methodology (see Appendix B) to estimate mass from the CPI measurements of projected area and aspect ratio. This new methodology assumes that ice particles with size less than $100 \mu\text{m}$ exhibit hexagonal column geometry. Such a geometrical assumption seems reasonable based on observations for sizes smaller than $100 \mu\text{m}$ (see Lawson et al., 2006, their Figs. 4 and 5), but it overestimates the mass for particles

Ice particle mass- and area-dimension expressions

E. Erfani and
D. L. Mitchell

[Title Page](#)[Abstract](#)[Introduction](#)[Conclusions](#)[References](#)[Tables](#)[Figures](#)[Back](#)[Close](#)[Full Screen / Esc](#)[Printer-friendly Version](#)[Interactive Discussion](#)

Ice particle mass- and area-dimension expressions

E. Erfani and
D. L. Mitchell

Title Page

Abstract

Introduction

Conclusions

References

Tables

Figures

◀

▶

◀

▶

Back

Close

Full Screen / Esc

Printer-friendly Version

Interactive Discussion



A curve fit based on SPARTICUS synoptic mean PSDs for $-40^{\circ}\text{C} < T \leq -20^{\circ}\text{C}$ is shown in Fig. 3 by the blue curve. This result differs markedly from previous studies where the relationship between $\log(m)$ and $\log(D)$ is linear, rather than a slowly varying curve as shown here. This finding is due to extending the range of ice particle size to smaller sizes, which was made possible by using data from the CPI probe. The m - D line corresponding to ice spheres is shown for reference since for a given D , the ice particle mass cannot exceed this value. Also shown is the curve fit for ice particle mass based on SCPP and CPI m - D measurements and estimates, respectively (the black curve). This SCPP data is described in detail in Sect. 4.1, but here it is sufficient to say that the 827 m - D measurements (with ice particle shapes corresponding to this temperature range) were grouped into size-intervals and the mean values within each size-interval are plotted in Fig. 3 (purple filled circles). The close agreement between the blue and black curves indicates that ice particle masses derived from 2D-S data are adequate surrogates for the SCPP m - D measurements. This agreement, mentioned in Sect. 2.1, forms part of the rationale for this study as described in that section.

To minimize variance, the mean PSDs were grouped into temperature categories and 2nd order polynomial curve fits were calculated for each category as shown in Table 1. The “goodness of fit” is given by the R^2 in Table 1, and the number of mean data points used is also indicated. Greater accuracy is obtained by using the fit equation for a specific temperature interval rather than using the fit equation corresponding to all temperatures sampled. The resulted curve fits are depicted in Fig. 4, where it is shown that for $T < -55^{\circ}\text{C}$, the m - D curves are considerably different for both synoptic and anvil cirrus relative to the warmer temperature intervals. It is also seen that the mean dependence of ice particle mass on particle size is not predicted to vary substantially between ice clouds of different type (i.e. synoptic vs. anvil) for a given temperature regime. The latter differs from the results of H2010, where they showed that m - D power laws for anvil ice clouds yield masses about a factor of two larger than for synoptic ice clouds. It is possible that the similarity in m - D expressions found here regarding

synoptic and anvil ice clouds is an artifact if ice particle volumes (for bulk ice) for a given A are quite different between cloud types.

The 2nd order polynomial A - D curve fits were provided in a similar way that m - D curve fits were obtained, and are shown in Table 2. An example of the mean PSD data and the polynomial A - D curve fit is shown in Fig. 5 for $-40^{\circ}\text{C} < T \leq -20^{\circ}\text{C}$. Again the PSD averaging process greatly reduces the spread in area for a given size. More scatter is seen at the largest sizes since the size bins here are populated by relatively few ice particles. The line for ice spheres indicates the maximum possible projected area for a given D . For each temperature interval, fractional uncertainties for each 2D-S size-bin were calculated as shown in Fig. 6 only for the temperature intervals having three or more PSDs. Fractional uncertainties are expressed as the σ of projected area divided by the mean projected area for each size-bin midpoint. Uncertainties are highly variable and range between 0 and 28 % of the mean bin A value, having a mean overall value of 11.0 %. Uncertainties tend to be zero for $D = 10\ \mu\text{m}$ since particles in this size bin (5–15 μm) generally shadow only one pixel in both vertical and time (horizontal) dimensions.

It is important to know whether the measured ice particle area and masses are internally consistent here since ice cloud properties like D_e and the mass-weighted fall speed (V_m) depend on the ice particle m/A ratio. The maximum value of the m/A ratio is given by an ice sphere. Thus a test for internal consistency is to calculate relative m/A , which is defined as:

$$R = \frac{\left(\frac{m}{A}\right)_{\text{particle}}}{\left(\frac{m}{A}\right)_{\text{sphere}}}. \quad (1)$$

This ratio should not exceed a value of 1.0. The data used to produce Tables 1 and 2 were tested in this way and this ratio never exceeded a value of 1.0. However, when curve fits provided only by 2D-S probe are used, this ratio exceeded the value of 1.0 for size less than 20 μm where A measurements are poorest. An example is shown in Fig. 7 for $-40^{\circ}\text{C} < T \leq -20^{\circ}\text{C}$. As shown by Heymsfield et al. (2002) and others,

Ice particle mass- and area-dimension expressions

E. Erfani and
D. L. Mitchell

Title Page

Abstract

Introduction

Conclusions

References

Tables

Figures



Back

Close

Full Screen / Esc

Printer-friendly Version

Interactive Discussion



Ice particle mass- and area-dimension expressions

E. Erfani and
D. L. Mitchell

Title Page

Abstract

Introduction

Conclusions

References

Tables

Figures



Back

Close

Full Screen / Esc

Printer-friendly Version

Interactive Discussion



common and often dominate N at smaller sizes (Korolev and Isaac, 2003; Lawson et al., 2006; C2012). The similarity between the hexagonal column m - D expression and the C2012 m - D expression in Fig. 1 suggests short hexagonal columns may serve as a proxy for compact irregular ice. Ice particles classified as unrimed having these shapes were used in Fig. 8, although some light riming is possible. The three main categories of ice particle shape are color-coded in Fig. 8, with columnar ice particles more common at small-to-intermediate sizes, side plane type ice particles more common at intermediate-to-large sizes, and bullet rosettes more common at intermediate sizes. The m - D curve fit, based on CPI and SCPP measurements, is from Table 1 for synoptic ice clouds for $-40^{\circ}\text{C} < T \leq -20^{\circ}\text{C}$.

Also shown are the recently published m - D power law relationships of C2012 and H2010 that were obtained from synoptic ($-60^{\circ}\text{C} < T < -20^{\circ}\text{C}$) and from both synoptic and anvil ($-60^{\circ}\text{C} < T < 0^{\circ}\text{C}$) ice clouds, respectively. These relationships are plotted over the size range used to produce them. The C2012 relationship consists of two lines and follows the curve fit remarkably well for $D > 100\ \mu\text{m}$, with differences never exceeding 50 %. The H2010 relationship consists of a single line and also approximates the curve fit well, except for $D < 100\ \mu\text{m}$ and $D > 1000\ \mu\text{m}$ where differences can reach about 100 %.

Figure 9 shows a polynomial curve fit based on mass estimates from the 2D-S (M7 processing) and CPI probes for sizes greater than $200\ \mu\text{m}$ and less than $100\ \mu\text{m}$, respectively. Also shown is SCPP data where the ice particle measurements were binned into size intervals of $100\ \mu\text{m}$ between 100 and $1000\ \mu\text{m}$, with subsequent intervals of 200 , 200 , 400 , 600 , 600 and $1000\ \mu\text{m}$ (up to $4\ \text{mm}$) at larger sizes to provide adequate sampling statistics. The σ within each size interval was calculated for m and D as shown by the vertical and horizontal red bars, respectively. The intersection point marks the mean value for m and D in each interval. The m - D curve fit for SPARTICUS synoptic ice clouds for $-40^{\circ}\text{C} < T \leq -20^{\circ}\text{C}$ is extrapolated to $4\ \text{mm}$ in Fig. 9 for comparison with the masses and sizes of these 827 ice particles sampled during SCPP. In this way, the SPARTICUS measurements roughly coincide with the temperatures of

Ice particle mass- and area-dimension expressions

E. Erfani and
D. L. Mitchell

Title Page

Abstract

Introduction

Conclusions

References

Tables

Figures

◀

▶

◀

▶

Back

Close

Full Screen / Esc

Printer-friendly Version

Interactive Discussion



from SPARTICUS data should be appropriate at colder temperatures if ice particle shape does not significantly change. Here we use the ice particle AR as a proxy for ice particle shape. The mean ice particle AR for each size-bin is shown for each 5 °C temperature interval in Figs. 10 and 11 for synoptic and anvil cirrus, respectively. ARs are similar among all temperature intervals excepting those for $T \leq -55$ °C. For $D > 60$ μm, these two coldest intervals exhibit ARs less than that for $T > -55$ °C in both synoptic and anvil ice clouds.

For purposes of calculating PSD A , m , and radar reflectivity (Z), the AR changes at these larger sizes are considered more critical than the AR changes at smaller sizes. It is therefore argued that for these applications, the noted methodology of obtaining m - D and A - D expressions from SPARTICUS data should be appropriate at colder temperatures down to -55 °C. For $T \leq -55$ °C, it appears that ice particle shape changes, and it is possible that the ice particle geometry changes in such a way that the BL2006 m - A expression is no longer valid. For example, if the BL2006 m - A expression implicitly assumes relatively compact ice particles growing in 3 dimensions, and the ice particle shape changes to planar crystals with 2-dimensional growth dominating, then the BL2006 m - A expression may perform poorly. We report m - D results for these coldest temperatures (Table 1), but with the caveat that these m - D expressions are highly uncertain. Additional research is needed to test these results. Moreover, this study addresses only mid-latitude synoptic and anvil ice clouds over land, and results may have been different if marine anvil cirrus, orographic cirrus and/or Arctic ice clouds were considered.

5 Uncertainties in m - D and A - D expressions

Conventional m - D and A - D expressions use power law relationships of the form:

$$m = \alpha D^\beta \quad (2)$$

$$A = \gamma D^\delta \quad (3)$$

to estimate ice particle mass and projected area, where α , β , γ and δ are constants. This study indicates that these terms should not be constants over all ice particle sizes, but that they can be approximated as constants over a range of particle size with good accuracy. The 2nd order polynomials used in this study have the form:

$$\ln x = a_0 + a_1 \ln D + a_2 (\ln D)^2 \quad (4)$$

where x is either m or A , and a_0 , a_1 and a_2 are constants. Differentiating Eq. (4) with respect to $\ln D$ gives the slope of this curve which is β for the mass case:

$$\frac{\partial(\ln m)}{\partial(\ln D)} = \beta = a_1 + 2a_2 \ln D. \quad (5)$$

Thus, β is a function of D , and for a given D , α can be solved for by equating the m - D power law (Eq. 2) with polynomial fit (Eq. 4):

$$\alpha = \frac{\exp \left[a_0 + a_1 \ln D + a_2 (\ln D)^2 \right]}{D^\beta}. \quad (6)$$

The same approach is used to solve for δ and γ for a given D . Uncertainties for the m - D and A - D polynomial fit expressions can be characterized by estimating σ for α and γ using field observations of m and A , and estimating σ for β and δ using selected values of D in the fit equations. This is possible due to the relatively low uncertainty in β and δ , as described below.

5.1 Uncertainties in the exponent of power law expressions

Values of β and δ are evaluated at five ice particle sizes and for all temperature intervals sampled for synoptic and anvil ice clouds, and are shown in Tables 3–6. For the two coldest temperature intervals, values are not shown for the two largest size categories since PSD did not extend to these sizes at these temperatures. The mean and

Ice particle mass- and area-dimension expressions

E. Erfani and
D. L. Mitchell

Title Page

Abstract

Introduction

Conclusions

References

Tables

Figures



Back

Close

Full Screen / Esc

Printer-friendly Version

Interactive Discussion



Ice particle mass- and area-dimension expressions

E. Erfani and
D. L. Mitchell

Title Page

Abstract

Introduction

Conclusions

References

Tables

Figures



Back

Close

Full Screen / Esc

Printer-friendly Version

Interactive Discussion



σ for β are calculated for each of the five ice particle sizes selected. Then, the mean uncertainty is expressed as a percent for the fraction mean σ /mean β that is averaged over all 5 selected sizes. This mean fractional uncertainty is the final uncertainty estimate for β and δ that can be applied for any size and temperature range. A key finding is that mean uncertainties for β do not exceed 9.1 % and mean uncertainties for δ do not exceed 8.5 %. This indicates that most of the scatter in measurements of ice particle mass and area can be attributed to uncertainties in α and γ , respectively.

Another interesting feature of Tables 3–6 is the evolution of β and δ with size. At the smallest sizes, ice particles tend to be quasi-spherical or isometric (Korolev and Isaac, 2003), with β and δ approaching values of 3 and 2, respectively, with decreasing size. As ice particles grow in size, they become more complex, often displaying branches in 3 dimensions (e.g. bullet rosettes and side planes). This produces less mass per unit length, and β and δ decrease. In Tables 5 and 6, δ is slightly greater than 2.00 (the maximum theoretical value) at the smallest size for some temperature intervals. This is likely due to inaccuracies in CPI projected area measurements at small sizes and an artifact of the curve-fitting process.

5.2 Uncertainties in prefactors of power law expressions

Figure 9 shows σ for SCPP m for each size interval. Since changes in β account for a relatively small portion of this uncertainty, to a first approximation we can attribute all this uncertainty to α . The percent uncertainty averaged over all sizes is calculated as the mean value of the fractional uncertainty of each size interval (σ /size-bin mean value), and is equal to ± 54.4 % for the mass σ values in Fig. 9. This is our estimate for the mean fractional σ for α for all ice clouds.

A similar analysis is needed for ice particle projected area, and for that we turn to the fractional uncertainty calculations shown in Fig. 6. The mean percent uncertainty for γ based on Fig. 6 is ± 11.2 %.

These mean σ values for α and γ should be representative σ estimates for the m - D and A - D expressions reported in this paper. Moreover, these uncertainties should be

using 2nd order polynomial fits may pose a quantum leap in model complexity. To avoid this problem, we propose the following treatment of m - D and A - D expressions.

To make this treatment practical for climate modeling, a procedure was developed that assumes advanced approximate knowledge of the PSD dimension of interest (D_i).

For example, if the ice cloud microphysical properties and processes being calculated are most relevant to the PSD mass moment (i.e. IWC), then the median mass dimension (D_m ; the particle size dividing the PSD mass into equal parts) is the D_i . Fortunately, 2-moment microphysical schemes in climate models provide such knowledge since the slope parameter (λ) of the PSD is predicted. The m - D exponent β is generally near 2 for $D > 150 \mu\text{m}$ (see Table 3 and 4) and tends to be ~ 2.7 for $D \sim 50 \mu\text{m}$. Thus, D_m can be approximated using an exact expression from Mitchell (1991):

$$D_m = \frac{\beta + \nu + 0.67}{\lambda} \quad (7)$$

where it assumes that a gamma function describes the PSD, given as:

$$N(D) = N_0 D^\nu \exp(-\lambda D) \quad (8)$$

and ν is the PSD dispersion parameter (often assumed to be constant) and N_0 depends on N or the IWC. Similarly, Tables 5 and 6 show δ is near 1.7 for $D > 150 \mu\text{m}$ and is close to 2.0 for $D \sim 50 \mu\text{m}$. If the PSD area moment is most relevant to model calculations (e.g. ice optical properties), then D_i is the median area dimension (D_A):

$$D_A = \frac{\delta + \nu + 0.67}{\lambda}. \quad (9)$$

Moreover, if the PSD radar reflectivity moment is most relevant to model calculations, then D_i is the median radar reflectivity dimension (D_Z):

$$D_Z = \frac{2\beta + \nu + 0.67}{\lambda}. \quad (10)$$

Ice particle mass- and area-dimension expressions

E. Erfani and
D. L. Mitchell

Title Page

Abstract

Introduction

Conclusions

References

Tables

Figures

◀

▶

◀

▶

Back

Close

Full Screen / Esc

Printer-friendly Version

Interactive Discussion



When addressing ice nucleation, either the mean size (\bar{D}) or the median number concentration dimension (D_N) may be used:

$$D_N = \frac{\nu + 0.67}{\lambda}. \quad (11)$$

Because β and δ vary slowly with respect to D , D_i can be well approximated for a given temperature regime by evaluating β and δ at $D = 500 \mu\text{m}$, and then solving for D_i . An iterative procedure can yield exact solutions for β , δ , α , γ , and D_i using the following steps: (a) β , δ , α , γ are evaluated at $D = 500 \mu\text{m}$ using Eqs. (5) and (6). (b) D_i is calculated as indicated above, along with any PSD properties of interest such as D_e or V_m . (c) β , δ , α , γ are recalculated based on D_i and the appropriate curve fit. (d) These updated values are then used to recalculate D_i , along with any PSD properties of interest. A single iteration yields D_A , D_m , δ and β within 0.5, 1.5, 0.6 and 1.9% of their exact values, respectively. Thus, only one iteration is needed for most applications since changes in D_i are primarily due to changes in λ .

Calculating D_i is a means of approximating the size range relevant to the ice properties or processes being determined. To calculate D_i , λ must be supplied by the cloud resolving model. In the Community Atmosphere Model version 5 (CAM5; Gettelman et al., 2010), λ is obtained from the ratio IWC/N where the PSD is expressed as a gamma function, as shown by Eq. (8). Solving for λ ,

$$\lambda = \left[\frac{\alpha \Gamma(\beta + \nu + 1) N}{\Gamma(\nu + 1) \text{IWC}} \right]^{\frac{1}{\beta}} \quad (12)$$

where Γ denotes the gamma function. Although the dependence of λ on α and β complicates matters, Eq. (12) can be solved iteratively using the following steps: (a) λ is initially estimated by evaluating α , β , γ and δ at $D = 500 \mu\text{m}$ for a given N and IWC using Eqs. (5), (6), and (12). (b) These values of λ , δ and β are then used to calculate D_i as described above. (c) The revised D_i value is then used in Eqs. (5) and (6) to

Ice particle mass- and area-dimension expressions

E. Erfani and
D. L. Mitchell

Title Page

Abstract

Introduction

Conclusions

References

Tables

Figures

⏪

⏩

◀

▶

Back

Close

Full Screen / Esc

Printer-friendly Version

Interactive Discussion



Ice particle mass- and area-dimension expressions

E. Erfani and
D. L. Mitchell

Title Page

Abstract

Introduction

Conclusions

References

Tables

Figures

◀

▶

◀

▶

Back

Close

Full Screen / Esc

Printer-friendly Version

Interactive Discussion



generate revised values for β , α , δ , and γ , which are then used in Eq. (12) to revise λ . (d) This revised λ revises D_i , and the cycle repeats but entering at step (c); subsequent iteration involves only steps (c) and (d). For solving Eq. (12), D_i is equal to D_m since the derivation of Eq. (12) reveals that α and β are associated with the IWC PSD moment.

5 Again, this approach is feasible since changes in λ primarily result from changes in N and IWC. The λ produced from a single iteration has an error of 1.2 % when $\bar{D} = 14 \mu\text{m}$ (in the size regime where errors are greatest).

Alternatively, λ can be obtained using a look-up table (LUT) that relates λ to N and IWC for all relevant combinations of α and β . The LUT can be produced through the iterative process described above.

10 While the resulting m - D or A - D power law is only valid over a limited size range, since it is centered on D_i , it should be sufficiently accurate for calculating various ice microphysical properties (some used to calculate optical properties) such as IWC, D_e , V_m , Z or ice nucleation rates. This also allows many microphysical rates and quantities to be represented analytically in a simple way since power law expressions are easily integrated over the PSD, and are thus compatible with climate model architectures. In this way, the m - D and A - D power laws become a function of the λ . This should significantly improve the accuracy of predicting cloud microphysical and radiative properties and cloud radiative forcing in general, and also unify microphysical and radiative processes under a common treatment of ice particle area and mass. It is noteworthy that a common data set is used to derive these m - D and A - D expressions, making them self-consistent (generally not achieved in past studies).

6.2 Impact on calculations of ice particle N , D_e , and V_m

25 First in this subsection, these quantities are calculated in the standard way, assuming constant values of α , β , γ and δ , and then they are calculated using the methodology explained in Sect. 6.1, where α , β , γ and δ exhibit a weak dependence on D . An exponential PSD is assumed ($\nu = 0$), and α , β , γ and δ are based on the warmest temperature regime ($-40^\circ\text{C} < T \leq -20^\circ\text{C}$).

variable ones. Also shown is D_e based on α , β , γ and δ values assumed for cloud ice in CAM5, which shows dramatic overestimation compared to two other methods, and these changes are greatest when $\bar{D} > 100 \mu\text{m}$.

The ice particle fall velocity (v_i) is another property that depends on the m/A ratio. The method of Heymsfield and Westbrook (2010) is sometimes used to predict v_i where v_i is predicted from the Best number (X), defined as:

$$X = \frac{\rho_{\text{air}}}{\eta^2} \frac{8mg}{\pi A_r^{0.5}} \quad (15)$$

where ρ_{air} is the density of air, η is the dynamic viscosity, g is the gravitational constant and A_r is the ice particle AR. The PSD V_m was calculated from D_m using the Heymsfield–Westbrook scheme, where α , β , γ and δ may be fixed or variable. Figure 14 denotes that considerable differences can exist for V_m at $\bar{D} < 20 \mu\text{m}$ and $\bar{D} > 500 \mu\text{m}$, depending on whether V_m was based on fixed or variable values of α , β , γ and δ . Note that V_m based on constant α , β , γ and δ is greater than V_m based on variable ones. In addition, V_m was calculated for the fixed values of α , β , γ and δ used in CAM5 for cloud ice. In this case, errors in V_m are much greater (with greatest error seen at $\bar{D} > 100 \mu\text{m}$), again underscoring potential errors that may result by assuming spheres for ice particles.

7 Conclusions and summary

The findings presented here constitute a fundamental shift in our way of representing ice particle mass and projected area in atmospheric models and remote sensing algorithms. Rather than having a multitude of m - D and A - D power law expressions for different ice particle shapes, size ranges, temperature regimes and/or cloud types, several 2nd order polynomial fits may suffice for ice clouds at different temperature intervals, perhaps only 3 for each cloud type (see Fig. 4). From these fit equations,

Ice particle mass- and area-dimension expressions

E. Erfani and
D. L. Mitchell

Title Page

Abstract

Introduction

Conclusions

References

Tables

Figures

◀

▶

◀

▶

Back

Close

Full Screen / Esc

Printer-friendly Version

Interactive Discussion



these fit equations relative to power laws having a fixed prefactor and exponent. Treating ice particles as spheres in cloud models was shown to produce large microphysical errors.

Remote sensing algorithms that retrieve cloud properties strongly depend on m - D and A - D power laws, with confidence levels for the retrieved cloud property often largely determined by the uncertainty associated with these power laws (e.g. Delanoë and Hogan, 2010). This study has quantified these uncertainties and has found that most of the uncertainty lies in the prefactor. Application of these m - D and A - D uncertainties to the remote sensing of ice cloud properties will likely improve the confidence of such retrievals. This study was focused only on mid-latitude continental ice clouds, and not on marine anvil or synoptic cirrus, orographic cirrus and/or Arctic ice clouds. The results might be different for these clouds, and additional research is required to test the approach introduced in this study in different environments.

Appendix A: Comparison between M1 and M7 methods for 2D-S probe

There are various methods to process 2D-S data, such as M1, M2, M4, and M7 methods (Lawson, 2011). Explanation and comparison of all these methods are beyond the scope of this paper. The M1 method was originally used in this study, but the newly developed M7 method was replaced for two main reasons. First, the M1 and M7 methods differ on the measurement of particle dimensions, as is shown in Fig. A1. The horizontal direction represents the direction of particle travel into the 2D-S probe and is sometimes referred to as the time dimension. The M1 method uses maximum dimension along the direction of travel (length scale $L1$) as the maximum dimension, whereas the M7 method uses the maximum dimension of the particle 2-D image (length scale $MaxLength$). Therefore, M7 method provides a more realistic measurement of maximum dimension. Length scale $L4$ in Fig. A1 is determined from the maximum number of shadowed photodiodes (vertical array) at any given instant.

Ice particle mass- and area-dimension expressions

E. Erfani and
D. L. Mitchell

Title Page

Abstract

Introduction

Conclusions

References

Tables

Figures



Back

Close

Full Screen / Esc

Printer-friendly Version

Interactive Discussion



Ice particle mass- and area-dimension expressions

E. Erfani and
D. L. Mitchell

Title Page

Abstract

Introduction

Conclusions

References

Tables

Figures

◀

▶

◀

▶

Back

Close

Full Screen / Esc

Printer-friendly Version

Interactive Discussion



Second, the M1 and M7 methods are distinct in the treatment of particles that intersect the edges of the 2D-S field of view. Using the M1 method, all particles are included in the measurement of projected area and number concentration, even particles that intersect the edges of the 2D-S field of view, and in those cases their maximum dimension and projected area is approximated. When using the M7 method, only particles that are completely inside the 2D-S field of view (“all-in” particles) are included. This provides an accurate measurement of projected area and maximum dimension for all particles. This difference is more pronounced in anvil cirrus clouds than in synoptic cirrus due to slightly larger ice particles in anvil clouds that have a greater chance of intersecting the edges of the 2D-S field of view.

Appendix B: Calculation of ice particle mass from CPI measurements of projected area and aspect ratio

There is no direct measurement of ice particle mass by the CPI probe. Moreover, the BL2006 m - A relationship is based on ice particles larger than $\sim 150 \mu\text{m}$. Therefore, we developed a new method for estimating mass based on CPI measurements of ice particle projected area, length and width. It is assumed that when $10 \mu\text{m} < D < 100 \mu\text{m}$, all ice crystals are hexagonal columns. The apparent aspect ratio (ε), defined as the CPI measured mean length-to-width ratio for a given size-interval, is generally between 1 and 2 in this size range and the ice crystals are known to be relatively dense (more mass per maximum dimension), making this shape assumption a reasonable approximation (Korolev and Isaac, 2003; Lawson et al., 2006; C2012). This is considerably more accurate than assuming ice particles to be spherical.

Figure B1 shows the geometrical features of a hexagonal prism that has eight faces: two basal faces with hexagonal shape and six prism faces with rectangular shape. The axis along the prism face is defined as the c axis and the maximum dimension across the basal face is defined as the a axis. The true aspect ratio (δ) of a hexagonal column is defined as $\frac{c}{a}$ (Lamb and Verlinde, 2011; Pruppacher and Klett, 1998). Since the CPI

$A_{p,max}$, and $\varepsilon = 1$ when $A = A_{b,max}$. So, the crystal orientation and apparent aspect ratio representing P2 and P3 will be the average of these two extremes $(\delta + 1)/2$. The overall value for ε should equal the average apparent aspect ratio corresponding to all three planes. Therefore, ε is equal to $[\delta + (\delta + 1)/2 + (\delta + 1)/2]/3$, and we can write:

$$\varepsilon = \frac{1}{3}(2\delta + 1). \quad (B4)$$

Solving for δ from Eq. (B4):

$$\delta = \frac{(3\varepsilon - 1)}{2}. \quad (B5)$$

Let A_{cpi} be the CPI measurement of projected area. Then, Eq. (B3) represents A_{cpi} , and it can be used to estimate a :

$$a \approx \left(\frac{3A_{cpi}}{2\delta + \frac{3^{\frac{3}{2}}}{8}} \right)^{\frac{1}{2}}. \quad (B6)$$

Volume of a hexagonal column (V) is defined as:

$$V = \left(\frac{3^{\frac{3}{2}}}{8} \right) a^2 c. \quad (B7)$$

The mass of a hexagonal column (m) is equal to $\rho_i V$ where ρ_i is bulk density of ice and is equal to 0.917 g cm^{-3} . Therefore, the ice particle mass can be estimated from a and δ as:

$$m_{cpi} = \rho_i \left(\frac{3^{\frac{3}{2}}}{8} \right) a^3 \delta. \quad (B8)$$

Since δ and a are calculated from Eqs. (B5) and (B6), respectively, m_{cpi} is estimated from A_{cpi} and ε .

**Ice particle mass-
and area-dimension
expressions**

E. Erfani and
D. L. Mitchell

Title Page	
Abstract	Introduction
Conclusions	References
Tables	Figures
◀	▶
◀	▶
Back	Close
Full Screen / Esc	
Printer-friendly Version	
Interactive Discussion	



Acknowledgement. This research was supported by the Office of Science (BER), US Department of Energy. We are very grateful to Paul Lawson, Sara Lance, Sarah Woods, Ted Fisher, and Qixu Mo for processing the SPARTICUS 2D-S and CPI data in a manner that best served the needs of this study. We are also grateful to Brad Baker for providing us with the measurements of ice particle projected area that were used in BL2006. The SCPP data used in this study and associated software is freely available to interested researchers; those interested should contact the second author.

References

- Bailey, M. P. and Hallett, J.: Growth rates and habits of ice crystals between -20° and -70°C , *J. Atmos. Sci.*, 61, 514–544, 2004.
- Bailey, M. P. and Hallett, J.: A comprehensive habit diagram for atmospheric ice crystals: confirmation from the laboratory, AIRS II, and other field studies, *J. Atmos. Sci.*, 66, 2888–2899, doi:10.1175/2009JAS2883.1, 2009.
- Baker, B. and Lawson, R. P.: Improvement in determination of ice water content from two-dimensional particle imagery, Part I: Image-to-mass relationships, *J. Appl. Meteorol. Clim.*, 45, 1282–1290, doi:10.1175/jam2398.1, 2006.
- Baran, A. J.: From the single-scattering properties of ice crystals to climate prediction: a way forward, *Atmos. Res.*, 112, 45–69, doi:10.1016/j.atmosres.2012.04.010, 2012.
- Brown, P. R. A. and Francis, P. N.: Improved measurements of the ice water content in cirrus using a total-water probe, *J. Atmos. Ocean. Tech.*, 12, 410–414, doi:10.1175/1520-0426(1995)012<0410:imotiw>2.0.co;2, 1995.
- Cotton, R. J., Field, P. R., Ulanowski, Z., Kaye, P. H., Hirst, E., Greenaway, R. S., Crawford, I., Crosier, J., and Dorsey, J.: The effective density of small ice particles obtained from in situ aircraft observations of mid-latitude cirrus, *Q. J. Roy. Meteor. Soc.*, 139, 1923–1934, doi:10.1002/qj.2058, 2013.
- Delanoe, J. and Hogan, R. J.: Combined CloudSat-CALIPSO-MODIS retrievals of the properties of ice clouds, *J. Geophys. Res.-Atmos.*, 115, D00h29, doi:10.1029/2009jd012346, 2010.
- Foot, J. S.: Some observations of the optical properties of clouds. Part II: Cirrus, *Q. J. Roy. Meteor. Soc.*, 114, 145–164, 1988.

Ice particle mass- and area-dimension expressions

E. Erfani and
D. L. Mitchell

Title Page

Abstract

Introduction

Conclusions

References

Tables

Figures



Back

Close

Full Screen / Esc

Printer-friendly Version

Interactive Discussion



Ice particle mass- and area-dimension expressions

E. Erfani and
D. L. Mitchell

Title Page

Abstract

Introduction

Conclusions

References

Tables

Figures

◀

▶

◀

▶

Back

Close

Full Screen / Esc

Printer-friendly Version

Interactive Discussion



Fu, Q.: An accurate parameterization of the solar radiative properties of cirrus clouds for climate models, *J. Climate*, 9, 2058–2082, doi:10.1175/1520-0442(1996)009<2058:aapots>2.0.co;2, 1996.

Fu, Q., Yang, P., and Sun, W. B.: An accurate parameterization of the infrared radiative properties of cirrus clouds for climate models, *J. Climate*, 11, 2223–2237, doi:10.1175/1520-0442(1998)011<2223:aapoti>2.0.co;2, 1998.

Gettelman, A., Liu, X., Ghan, S. J., Morrison, H., Park, S., Conley, A. J., Klein, S. A., Boyle, J., Mitchell, D. L., and Li, J. L. F.: Global simulations of ice nucleation and ice supersaturation with an improved cloud scheme in the Community Atmosphere Model, *J. Geophys. Res.-Atmos.*, 115, D18216, doi:10.1029/2009jd013797, 2010.

Heymsfield, A. J. and Westbrook, C. D.: Advances in the estimation of ice particle fall speeds using laboratory and field measurements, *J. Atmos. Sci.*, 67, 2469–2482, doi:10.1175/2010jas3379.1, 2010.

Heymsfield, A. J., Lewis, S., Bansemer, A., Iaquina, J., Miloshevich, L. M., Kajikawa, M., Twohy, C., and Poellot, M. R.: A general approach for deriving the properties of cirrus and stratiform ice cloud particles, *J. Atmos. Sci.*, 59, 3–29, doi:10.1175/1520-0469(2002)059<0003:agafdt>2.0.co;2, 2002.

Heymsfield, A. J., Bansemer, A., Schmitt, C., Twohy, C., and Poellot, M. R.: Effective ice particle densities derived from aircraft data, *J. Atmos. Sci.*, 61, 982–1003, doi:10.1175/1520-0469(2004)061<0982:eipddf>2.0.co;2, 2004.

Heymsfield, A. J., Bansemer, A., and Twohy, C. H.: Refinements to ice particle mass dimensional and terminal velocity relationships for ice clouds. Part I: Temperature dependence, *J. Atmos. Sci.*, 64, 1047–1067, doi:10.1175/jas3890.1, 2007.

Heymsfield, A. J., Schmitt, C., Bansemer, A., and Twohy, C. H.: Improved representation of ice particle masses based on observations in natural clouds, *J. Atmos. Sci.*, 67, 3303–3318, doi:10.1175/2010jas3507.1, 2010.

Korolev, A.: Reconstruction of the sizes of spherical particles from their shadow images, Part I: Theoretical considerations, *J. Atmos. Ocean. Tech.*, 24, 376–389, doi:10.1175/jtech1980.1, 2007.

Korolev, A. and Isaac, G.: Roundness and aspect ratio of particles in ice clouds, *J. Atmos. Sci.*, 60, 1795–1808, doi:10.1175/1520-0469(2003)060<1795:raarop>2.0.co;2, 2003.

**Ice particle mass-
and area-dimension
expressions**E. Erfani and
D. L. Mitchell

Title Page

Abstract

Introduction

Conclusions

References

Tables

Figures



Back

Close

Full Screen / Esc

Printer-friendly Version

Interactive Discussion



Korolev, A., Strapp, J. W., and Isaac, G. A.: Evaluation of the accuracy of PMS optical array probes, *J. Atmos. Ocean. Tech.*, 15, 708–720, doi:10.1175/1520-0426(1998)015<0708:eotaop>2.0.co;2, 1998.

Lamb, D. and Verlinde, J.: *Physics and Chemistry of Clouds*, Cambridge University Press, New York, NY, USA, 2011.

Lawson, R. P.: Effects of ice particles shattering on the 2D-S probe, *Atmos. Meas. Tech.*, 4, 1361–1381, doi:10.5194/amt-4-1361-2011, 2011.

Lawson, R. P., Baker, B. A., Schmitt, C. G., and Jensen, T. L.: An overview of microphysical properties of Arctic clouds observed in May and July 1998 during FIRE ACE, *J. Geophys. Res.-Atmos.*, 106, 14989–15014, doi:10.1029/2000jd900789, 2001.

Lawson, R. P., O'Connor, D., Zmarzly, P., Weaver, K., Baker, B., Mo, Q., and Jons-son, H.: The 2D-S (Stereo) probe: design and preliminary tests of a new airborne, high-speed, high-resolution particle Imaging probe, *J. Atmos. Ocean. Tech.*, 23, 1462–1477, doi:10.1175/jtech1927.1, 2006.

Lawson, R. P., Jensen, E., Mitchell, D. L., Baker, B., Mo, Q., and Pilon, B.: Microphysical and radiative properties of tropical clouds investigated in TC4 and NAMMA, *J. Geophys. Res.-Atmos.*, 115, D00j08, doi:10.1029/2009jd013017, 2010.

Mace, J., Jensen, E., McFarquhar, G., Comstock, J., Ackerman, T., Mitchell, D., Liu, X., and Garrett, T.: SPARTICUS: small Particles in Cirrus, Science and Operations Plan, Tech. Rep., DOE/SC-ARM-10–003, The Atmospheric Radiation Measurement Program, US Department of Energy, available at: <https://www.arm.gov/publications/programdocs/doe-sc-arm-10-003.pdf> (last access: 20 October 2015), 2009.

Mishra, S., Mitchell, D. L., Turner, D. D., and Lawson, R. P.: Parameterization of ice fall speeds in midlatitude cirrus: results from SPARTICUS, *J. Geophys. Res.-Atmos.*, 119, 3857–3876, doi:10.1002/2013jd020602, 2014.

Mitchell, D. L.: Evolution of snow-size spectra in cyclonic storms, 1. Snow growth by vapor-deposition and aggregation, *J. Atmos. Sci.*, 45, 3431–3452, doi:10.1175/1520-0469(1988)045<3431:eosssi>2.0.co;2, 1988.

Mitchell, D. L.: Evolution of snow-size spectra in cyclonic storms, 2. Deviations from the exponential form, *J. Atmos. Sci.*, 48, 1885–1899, doi:10.1175/1520-0469(1991)048<1885:eosssi>2.0.co;2, 1991.

**Ice particle mass-
and area-dimension
expressions**E. Erfani and
D. L. Mitchell[Title Page](#)[Abstract](#)[Introduction](#)[Conclusions](#)[References](#)[Tables](#)[Figures](#)[Back](#)[Close](#)[Full Screen / Esc](#)[Printer-friendly Version](#)[Interactive Discussion](#)

Mitchell, D. L.: Use of mass- and area-dimensional power laws for determining precipitation particle terminal velocities, *J. Atmos. Sci.*, 53, 1710–1723, doi:10.1175/1520-0469(1996)053<1710:uomaad>2.0.co;2, 1996.

Mitchell, D. L.: Parameterization of the Mie extinction and absorption coefficients for water clouds, *J. Atmos. Sci.*, 57, 1311–1326, doi:10.1175/1520-0469(2000)057<1311:potmea>2.0.co;2, 2000.

Mitchell, D. L.: Effective diameter in radiation transfer: general definition, applications, and limitations, *J. Atmos. Sci.*, 59, 2330–2346, doi:10.1175/1520-0469(2002)059<2330:edirtg>2.0.co;2, 2002.

Mitchell, D. L., Zhang, R., and Pitter, R. L.: Mass-dimensional relationships for ice particles and the influence of riming on snowfall rates, *J. Appl. Meteorol.*, 29, 153–163, doi:10.1175/1520-0450(1990)029<0153:mdrfip>2.0.co;2, 1990.

Mitchell, D. L., Baran, A. J., Arnott, W. P., and Schmitt, C.: Testing and comparing the modified anomalous diffraction approximation, *J. Atmos. Sci.*, 63, 2948–2962, doi:10.1175/jas3775.1, 2006.

Mitchell, D. L., Rasch, P., Ivanova, D., McFarquhar, G., and Nousiainen, T.: Impact of small ice crystal assumptions on ice sedimentation rates in cirrus clouds and GCM simulations, *Geophys. Res. Lett.*, 35, L09806, doi:10.1029/2008gl033552, 2008.

Mitchell, D. L., d'Entremont, R. P., and Lawson, R. P.: Inferring cirrus size distributions through satellite remote sensing and microphysical databases, *J. Atmos. Sci.*, 67, 1106–1125, doi:10.1175/2009jas3150.1, 2010.

Mitchell, D. L., Mishra, S., and Lawson, R. P.: Representing the ice fall speed in climate models: results from tropical composition, cloud and climate coupling (TC4) and the indirect and semi-direct aerosol campaign (ISDAC), *J. Geophys. Res.-Atmos.*, 116, D00t03, doi:10.1029/2010jd015433, 2011.

Morrison, H. and Gettelman, A.: A new two-moment bulk stratiform cloud microphysics scheme in the community atmosphere model, version 3 (CAM3), Part I: Description and numerical tests, *J. Climate*, 21, 3642–3659, doi:10.1175/2008jcli2105.1, 2008.

Pruppacher, H. R. and Klett, J. D.: *Microphysics of Clouds and Precipitation*, 2nd edn., Kluwer Academic Publishers, Dordrecht, the Netherlands, 1996.

Sanderson, B. M., Piani, C., Ingram, W. J., Stone, D. A., and Allen, M. R.: Towards constraining climate sensitivity by linear analysis of feedback patterns in thousands of perturbed-physics GCM simulations, *Clim. Dynam.*, 30, 175–190, doi:10.1007/s00382-007-0280-7, 2008.

Yang, P., Wei, H. L., Huang, H. L., Baum, B. A., Hu, Y. X., Kattawar, G. W., Mishchenko, M. I., and Fu, Q.: Scattering and absorption property database for nonspherical ice particles in the near- through far-infrared spectral region, *Appl. Optics*, 44, 5512–5523, doi:10.1364/ao.44.005512, 2005.

- 5 Zhao, Y., Mace, G. G., and Comstock, J. M.: The occurrence of particle size distribution bimodality in midlatitude cirrus as inferred from ground-based remote sensing data, *J. Atmos. Sci.*, 68, 1162–1177, doi:10.1175/2010jas3354.1, 2011.

ACPD

15, 28517–28573, 2015

**Ice particle mass-
and area-dimension
expressions**E. Erfani and
D. L. Mitchell

Title Page

Abstract

Introduction

Conclusions

References

Tables

Figures

◀

▶

◀

▶

Back

Close

Full Screen / Esc

Printer-friendly Version

Interactive Discussion



Ice particle mass-
and area-dimension
expressionsE. Erfani and
D. L. Mitchell

Table 1. Polynomial curve fits of the form $\ln m = a_0 + a_1 \ln D + a_2 (\ln D)^2$ for synoptic and anvil cirrus clouds sampled during SPARTICUS, where m is in g and D is in cm. The only exception is for synoptic cirrus between -20 and -40 °C, where SCPP data was used in lieu of SPARTICUS data, as shown in Fig. 3. The number of m - D samples is given by N , along with the coefficient of determination (R^2) of the curve fit. See Sect. 3 for details.

Temperature Range	a_0	a_1	a_2	N	R^2
Synoptic Cirrus Clouds					
-40 °C $< T \leq -20$ °C	-6.72924	1.17421	-0.15980	201	0.99702
-55 °C $< T \leq -40$ °C	-7.21010	1.26123	-0.12184	139	0.99507
-65 °C $< T \leq -55$ °C	-11.34570	-0.45436	-0.29627	54	0.99283
Anvil Cirrus Clouds					
-40 °C $< T \leq -20$ °C	-6.67252	1.36857	-0.12293	226	0.99773
-55 °C $< T \leq -40$ °C	-6.44787	1.64429	-0.07788	160	0.98368
-65 °C $< T \leq -55$ °C	-9.24318	0.57189	-0.17865	49	0.98285

Title Page

Abstract

Introduction

Conclusions

References

Tables

Figures

◀

▶

◀

▶

Back

Close

Full Screen / Esc

Printer-friendly Version

Interactive Discussion



Ice particle mass-
and area-dimension
expressionsE. Erfani and
D. L. Mitchell**Table 2.** Polynomial curve fits of the form $\ln A = a_0 + a_1 \ln D + a_2 (\ln D)^2$ for synoptic and anvil cirrus clouds sampled during SPARTICUS, where A is in cm^2 and D is in cm. The number of A - D samples is given by N , along with the coefficient of determination (R^2) of the curve fit.

Temperature Range	a_0	a_1	a_2	N	R^2
Synoptic Cirrus Clouds					
$-40^\circ\text{C} < T \leq -20^\circ\text{C}$	-2.46356	1.25892	-0.07845	201	0.99803
$-55^\circ\text{C} < T \leq -40^\circ\text{C}$	-2.60478	1.32260	-0.05957	139	0.99781
$-65^\circ\text{C} < T \leq -55^\circ\text{C}$	-4.63488	0.54233	-0.13260	54	0.99784
Anvil Cirrus Clouds					
$-40^\circ\text{C} < T \leq -20^\circ\text{C}$	-2.40314	1.29749	-0.07233	226	0.99852
$-55^\circ\text{C} < T \leq -40^\circ\text{C}$	-2.38913	1.40166	-0.05219	160	0.99753
$-65^\circ\text{C} < T \leq -55^\circ\text{C}$	-2.43451	1.60639	-0.01164	49	0.98606

Title Page

Abstract

Introduction

Conclusions

References

Tables

Figures

◀

▶

◀

▶

Back

Close

Full Screen / Esc

Printer-friendly Version

Interactive Discussion



Ice particle mass- and area-dimension expressions

E. Erfani and
D. L. Mitchell

Title Page

Abstract

Introduction

Conclusions

References

Tables

Figures

◀

▶

◀

▶

Back

Close

Full Screen / Esc

Printer-friendly Version

Interactive Discussion



Table 3. Uncertainty estimates for mass-dimension power β for synoptic cirrus clouds.

Temperature Range	Ice Particle Size (μm)				
	50	150	500	1500	4500
	Power β				
$-25^\circ\text{C} < T \leq -20^\circ\text{C}$	2.792	2.455	2.085	1.748	1.411
$-30^\circ\text{C} < T \leq -25^\circ\text{C}$	2.846	2.449	2.015	1.618	1.221
$-35^\circ\text{C} < T \leq -30^\circ\text{C}$	2.773	2.429	2.053	1.710	1.367
$-40^\circ\text{C} < T \leq -35^\circ\text{C}$	2.642	2.371	2.073	1.802	1.530
$-45^\circ\text{C} < T \leq -40^\circ\text{C}$	2.556	2.254	1.923	1.621	1.320
$-50^\circ\text{C} < T \leq -45^\circ\text{C}$	2.549	2.276	1.977	1.704	1.431
$-55^\circ\text{C} < T \leq -50^\circ\text{C}$	2.495	2.322	2.133	1.960	1.787
$-60^\circ\text{C} < T \leq -55^\circ\text{C}$	2.686	2.064	1.382	–	–
$-65^\circ\text{C} < T \leq -60^\circ\text{C}$	2.863	1.732	–	–	–
Mean β	2.689	2.261	1.955	1.738	1.438
Standard Deviation of β	0.129	0.220	0.225	0.109	0.168
Mean Uncertainty (%)	9.031				

Ice particle mass-
and area-dimension
expressionsE. Erfani and
D. L. Mitchell

Title Page

Abstract

Introduction

Conclusions

References

Tables

Figures

◀

▶

◀

▶

Back

Close

Full Screen / Esc

Printer-friendly Version

Interactive Discussion

**Table 4.** Same as Table 3, but for anvil cirrus clouds.

Temperature Range	Ice Particle Size (μm)				
	50	150	500	1500	4500
	Power β				
$-25^\circ\text{C} < T \leq -20^\circ\text{C}$	2.614	2.387	2.138	1.911	1.683
$-30^\circ\text{C} < T \leq -25^\circ\text{C}$	2.726	2.426	2.098	1.799	1.499
$-35^\circ\text{C} < T \leq -30^\circ\text{C}$	2.653	2.394	2.110	1.850	1.591
$-40^\circ\text{C} < T \leq -35^\circ\text{C}$	2.679	2.394	2.083	1.798	1.513
$-45^\circ\text{C} < T \leq -40^\circ\text{C}$	2.655	2.370	2.058	1.773	1.488
$-50^\circ\text{C} < T \leq -45^\circ\text{C}$	2.531	2.302	2.051	1.822	1.593
$-55^\circ\text{C} < T \leq -50^\circ\text{C}$	2.432	2.273	2.100	1.941	1.782
$-60^\circ\text{C} < T \leq -55^\circ\text{C}$	2.533	2.105	1.637	–	–
$-65^\circ\text{C} < T \leq -60^\circ\text{C}$	2.446	1.956	1.419	–	–
Mean β	2.585	2.290	1.966	1.842	1.593
Standard Deviation of β	0.105	0.159	0.255	0.063	0.108
Mean Uncertainty (%)	6.715				

Ice particle mass-
and area-dimension
expressionsE. Erfani and
D. L. Mitchell**Table 5.** Uncertainty estimates for area-dimension power δ for synoptic cirrus clouds.

Temperature Range	Ice Particle Size (μm)				
	50	150	500	1500	4500
	Power δ				
$-25^\circ\text{C} < T \leq -20^\circ\text{C}$	2.133	1.938	1.725	1.531	1.337
$-30^\circ\text{C} < T \leq -25^\circ\text{C}$	2.170	1.932	1.671	1.432	1.194
$-35^\circ\text{C} < T \leq -30^\circ\text{C}$	2.140	1.927	1.693	1.480	1.267
$-40^\circ\text{C} < T \leq -35^\circ\text{C}$	2.027	1.882	1.722	1.576	1.431
$-45^\circ\text{C} < T \leq -40^\circ\text{C}$	2.011	1.821	1.612	1.422	1.232
$-50^\circ\text{C} < T \leq -45^\circ\text{C}$	1.941	1.810	1.666	1.534	1.403
$-55^\circ\text{C} < T \leq -50^\circ\text{C}$	1.861	1.842	1.821	1.801	1.782
$-60^\circ\text{C} < T \leq -55^\circ\text{C}$	1.960	1.669	1.350	–	–
$-65^\circ\text{C} < T \leq -60^\circ\text{C}$	2.018	1.509	–	–	–
Mean δ	2.029	1.814	1.658	1.540	1.378
Standard Deviation of δ	0.103	0.142	0.138	0.128	0.198
Mean Uncertainty (%)	8.428				

Title Page

Abstract

Introduction

Conclusions

References

Tables

Figures

◀

▶

◀

▶

Back

Close

Full Screen / Esc

Printer-friendly Version

Interactive Discussion



Ice particle mass-
and area-dimension
expressionsE. Erfani and
D. L. Mitchell**Table 6.** Same as Table 5, but for anvil cirrus clouds.

Temperature Range	Ice Particle Size (μm)				
	50	150	500	1500	4500
	Power δ				
$-25^\circ\text{C} < T \leq -20^\circ\text{C}$	2.023	1.899	1.763	1.639	1.515
$-30^\circ\text{C} < T \leq -25^\circ\text{C}$	2.108	1.925	1.724	1.541	1.357
$-35^\circ\text{C} < T \leq -30^\circ\text{C}$	2.051	1.900	1.735	1.584	1.434
$-40^\circ\text{C} < T \leq -35^\circ\text{C}$	2.063	1.894	1.708	1.539	1.370
$-45^\circ\text{C} < T \leq -40^\circ\text{C}$	2.055	1.885	1.698	1.528	1.358
$-50^\circ\text{C} < T \leq -45^\circ\text{C}$	1.943	1.828	1.701	1.586	1.470
$-55^\circ\text{C} < T \leq -50^\circ\text{C}$	1.869	1.808	1.740	1.679	1.618
$-60^\circ\text{C} < T \leq -55^\circ\text{C}$	1.760	1.753	1.746	–	–
$-65^\circ\text{C} < T \leq -60^\circ\text{C}$	1.754	1.561	1.350	–	–
Mean δ	1.959	1.828	1.685	1.585	1.446
Standard Deviation of δ	0.135	0.114	0.128	0.056	0.097
Mean Uncertainty (%)	6.233				

Title Page

Abstract

Introduction

Conclusions

References

Tables

Figures

◀

▶

◀

▶

Back

Close

Full Screen / Esc

Printer-friendly Version

Interactive Discussion



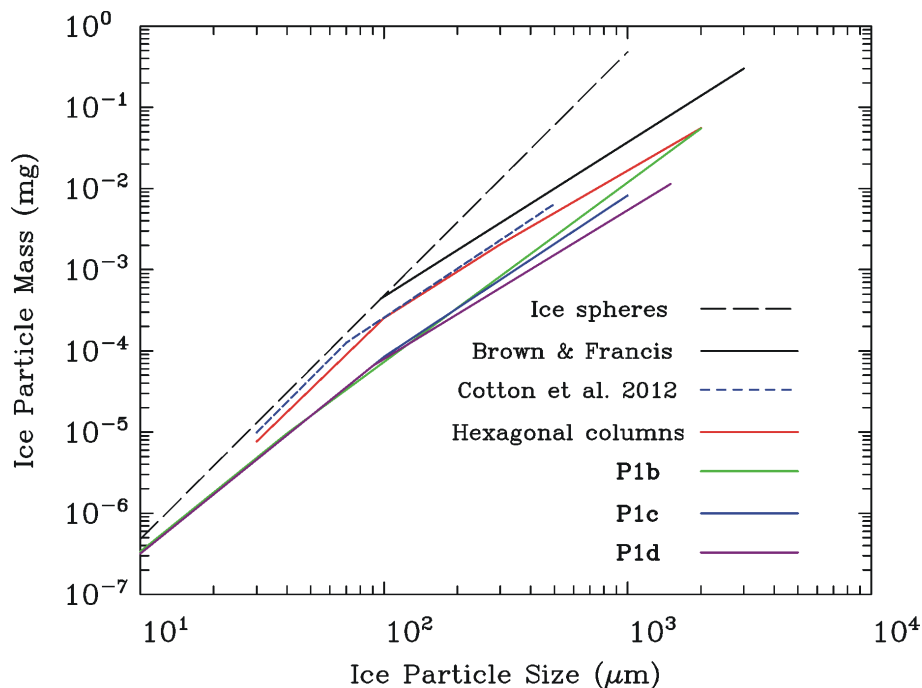
Ice particle mass-
and area-dimension
expressionsE. Erfani and
D. L. Mitchell

Figure 1. Dependence of ice particle mass (m) on ice particle maximum dimension (D), based on a variety of power law relationships in the literature (see text for details). Ice spheres indicate an upper limit for m at a given D . P1b, P1c and P1d denote planar crystals with sectorlike branches, broad branches and stellar dendrites, respectively, as described in Mitchell (1996).

Title Page

Abstract

Introduction

Conclusions

References

Tables

Figures

◀

▶

◀

▶

Back

Close

Full Screen / Esc

Printer-friendly Version

Interactive Discussion



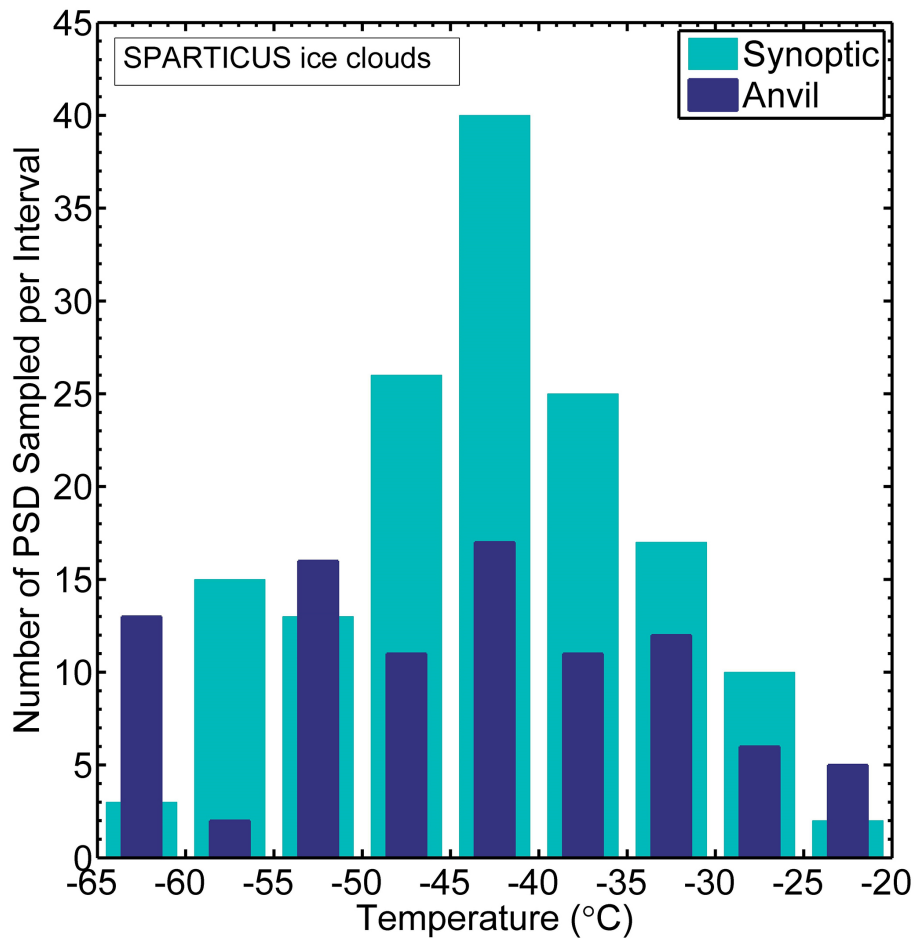


Figure 2. SPARTICUS PSD sampling statistics for synoptic and anvil cirrus clouds where the PSDs have been grouped into temperature intervals of 5°C.

**Ice particle mass-
and area-dimension
expressions**

E. Erfani and
D. L. Mitchell

Title Page

Abstract Introduction

Conclusions References

Tables Figures

◀ ▶

◀ ▶

Back Close

Full Screen / Esc

Printer-friendly Version

Interactive Discussion



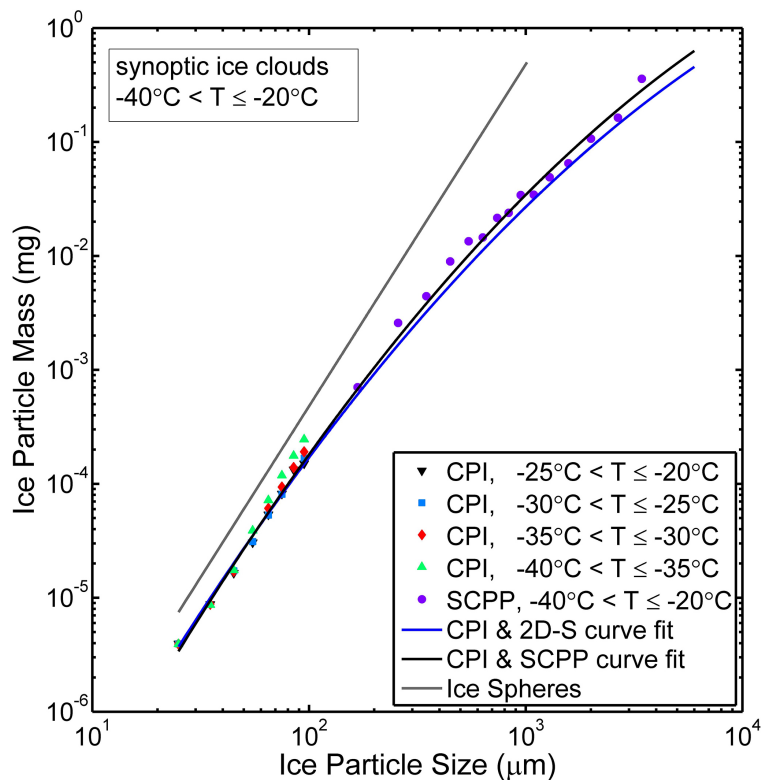


Figure 3. Dependence of ice particle mass on D for mean PSDs sampled from synoptic cirrus clouds during SPARTICUS for $-40^{\circ}\text{C} < T = -20^{\circ}\text{C}$ (blue curve fit based on CPI and 2D-S data), where a single mean PSD is the mean of all PSD contained within a 5°C temperature interval. Also shown are CPI and SCPP data that are grouped into size-bins for the indicated temperature ranges and the black curve fit based on these data (see Table 1 for equation). The grey line for ice spheres gives the maximum possible mass for a given D .

Ice particle mass and area-dimension expressions

E. Erfani and
D. L. Mitchell

Title Page

Abstract

Introduction

Conclusions

References

Tables

Figures

◀

▶

◀

▶

Back

Close

Full Screen / Esc

Printer-friendly Version

Interactive Discussion



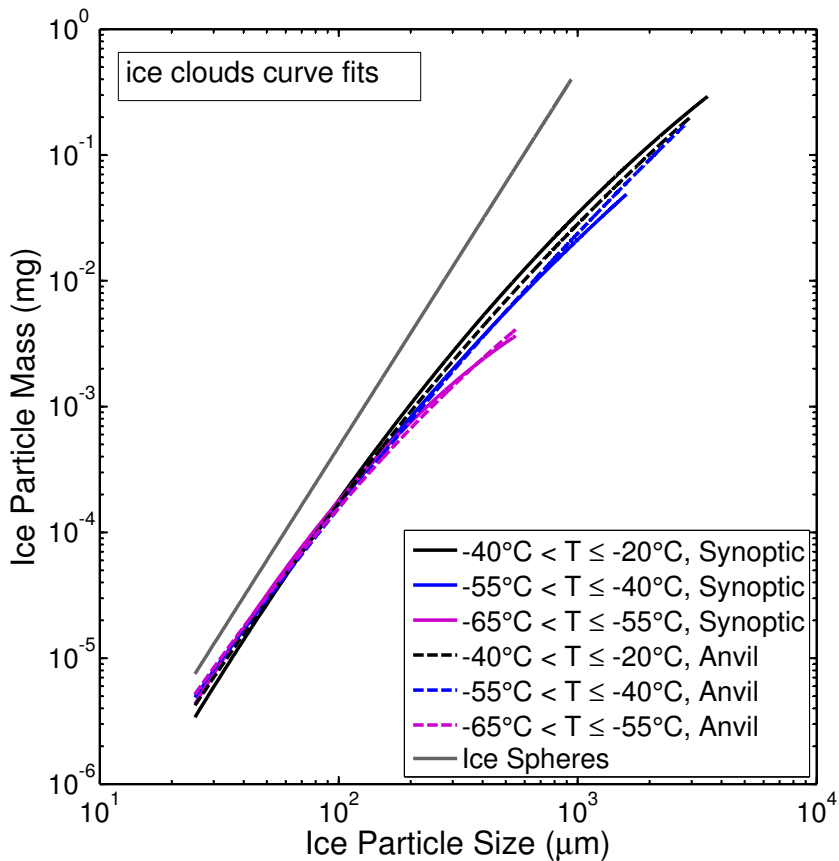


Figure 4. Comparison of all the curve fits in Table 1 for each temperature regime (indicated by color) and cloud type (indicated by line type; solid or dashed). The anvil and synoptic curve fits are very similar.

**Ice particle mass-
and area-dimension
expressions**

E. Erfani and
D. L. Mitchell

Title Page

Abstract

Introduction

Conclusions

References

Tables

Figures

◀

▶

◀

▶

Back

Close

Full Screen / Esc

Printer-friendly Version

Interactive Discussion



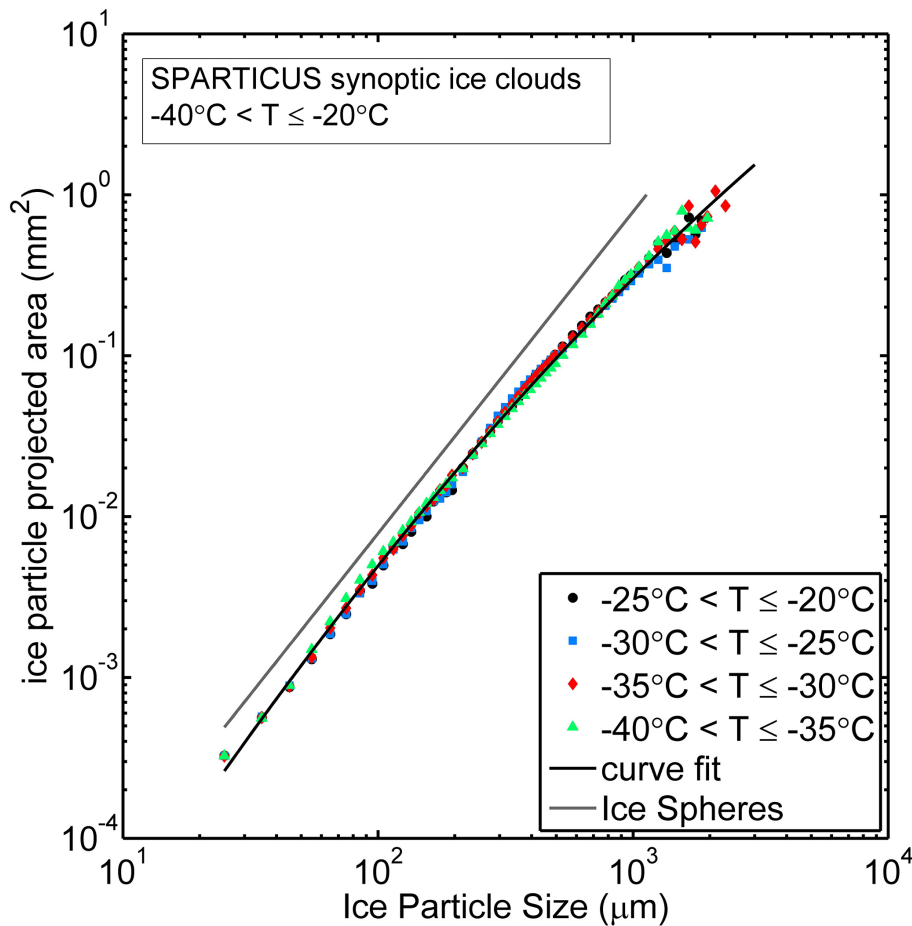
Ice particle mass-
and area-dimension
expressionsE. Erfani and
D. L. Mitchell

Figure 5. Dependence of ice particle projected area (A) on D based on mean PSD within the indicated temperature regime. The CPI and 2D-S data have been grouped into size-bins, and the black solid curve is a fit to these datasets (see Table 2 for equation).

Title Page

Abstract

Introduction

Conclusions

References

Tables

Figures

◀

▶

◀

▶

Back

Close

Full Screen / Esc

Printer-friendly Version

Interactive Discussion



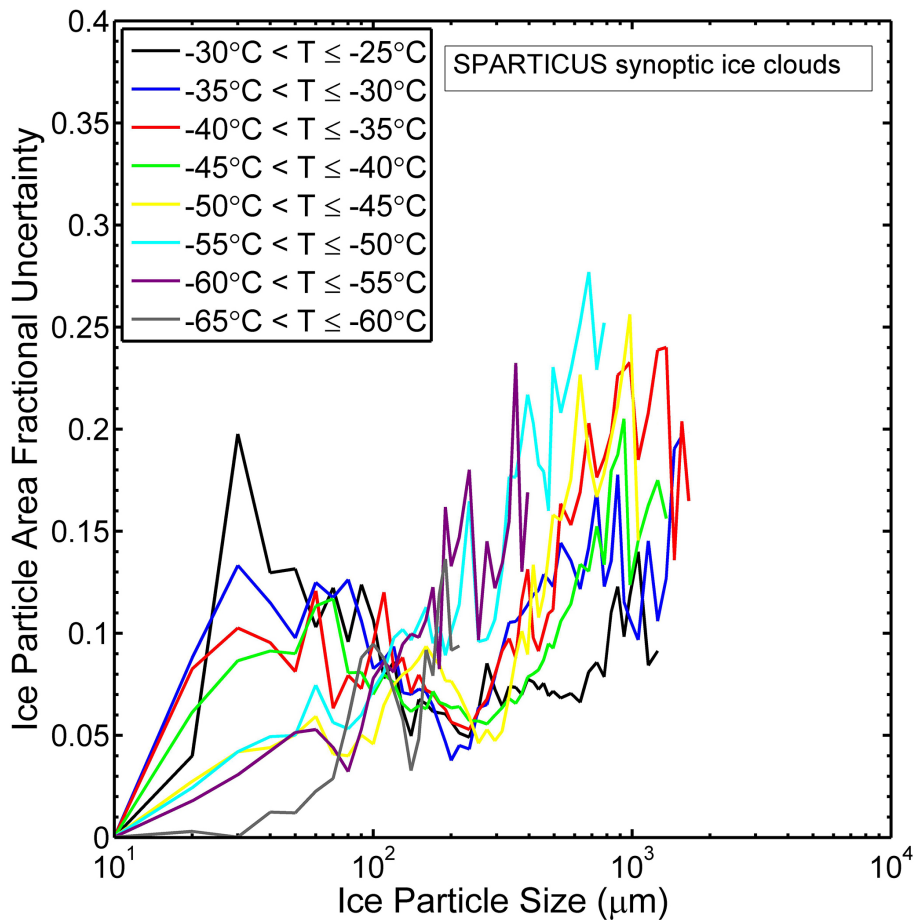


Figure 6. Fractional uncertainties (standard deviation/mean) for the mean ice particle projected area in each bin of the measured PSDs. Only temperature intervals having more than two PSDs are considered.

Ice particle mass- and area-dimension expressions

E. Erfani and
D. L. Mitchell

Title Page

Abstract

Introduction

Conclusions

References

Tables

Figures



Back

Close

Full Screen / Esc

Printer-friendly Version

Interactive Discussion



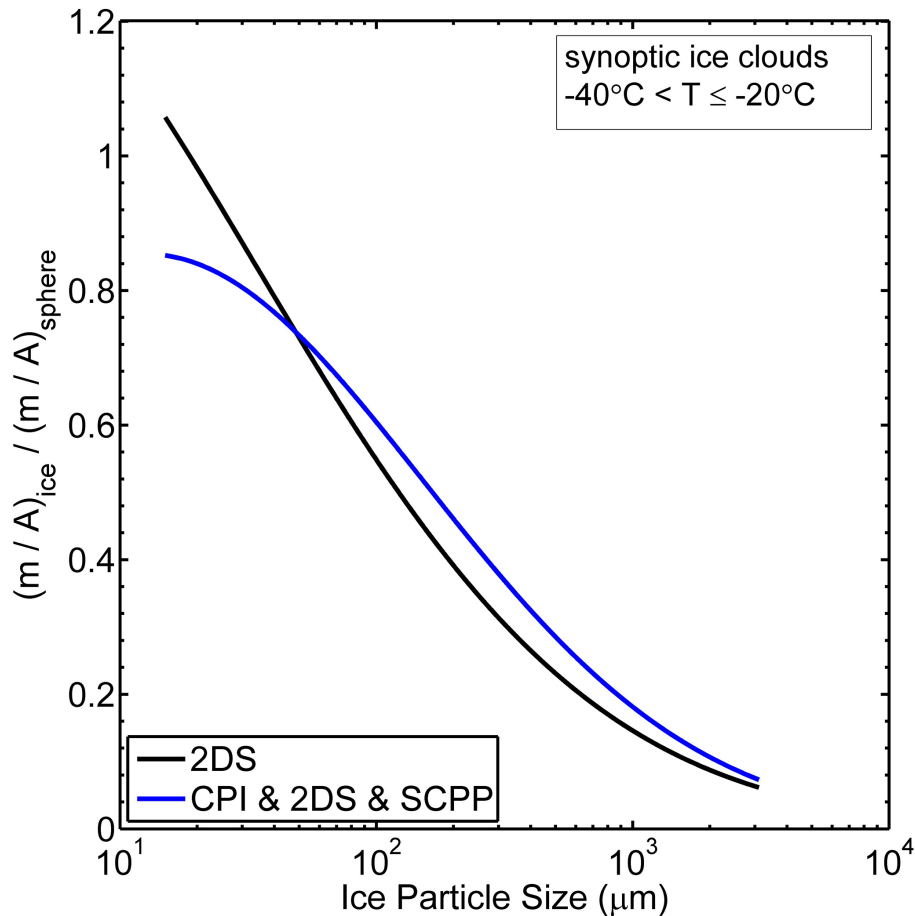


Figure 7. The m/A ratio for ice particles normalized by the corresponding m/A ratio for ice spheres using the $m-D$ and $A-D$ curve fits appropriate for the indicated temperature regime. Blue curve is based on Tables 1 and 2, but black curve is only based on 2D-S data.

**Ice particle mass-
and area-dimension
expressions**

E. Erfani and
D. L. Mitchell

Title Page	
Abstract	Introduction
Conclusions	References
Tables	Figures
◀	▶
◀	▶
Back	Close
Full Screen / Esc	
Printer-friendly Version	
Interactive Discussion	



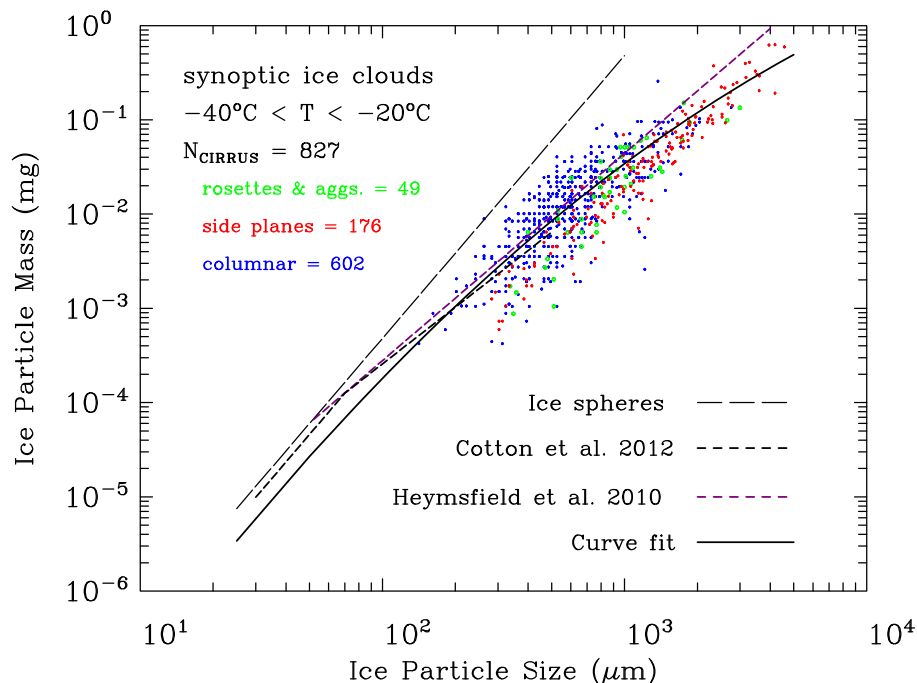
Ice particle mass-
and area-dimension
expressionsE. Erfani and
D. L. Mitchell

Figure 8. The m - D curve fit based on SCPP and CPI data (for indicated temperature regime) is compared with individual ice particle m - D measurements from SCPP, corresponding to ice particle shapes originating from similar temperatures. The number of ice particles sampled in each shape category is indicated. Also shown are comparisons with two other studies that derived m - D power laws from ice cloud field data.

Title Page

Abstract

Introduction

Conclusions

References

Tables

Figures

◀

▶

◀

▶

Back

Close

Full Screen / Esc

Printer-friendly Version

Interactive Discussion

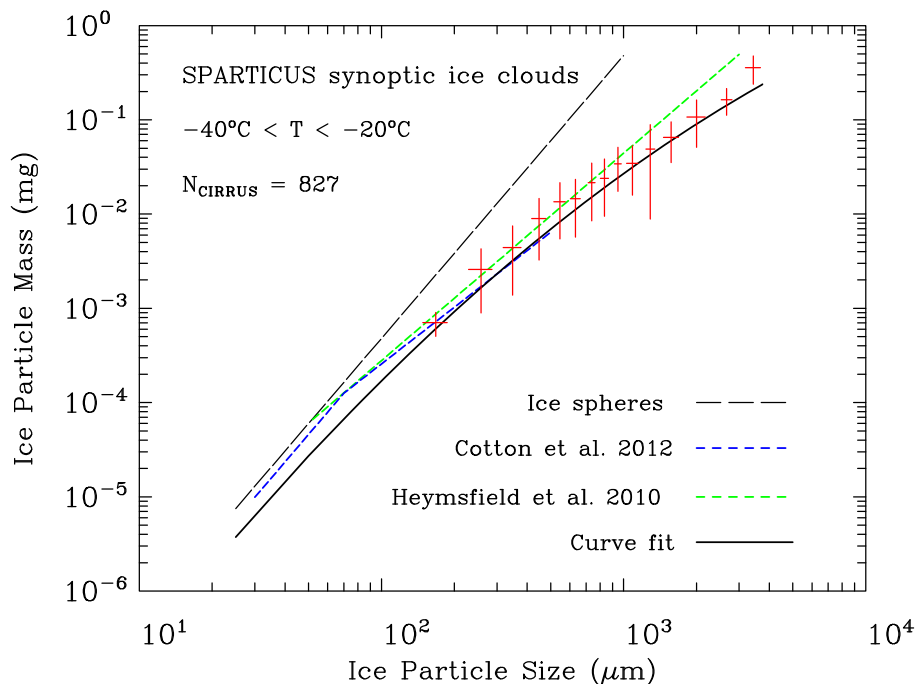
Ice particle mass-
and area-dimension
expressionsE. Erfani and
D. L. Mitchell

Figure 9. Same as Fig. 8, except the m - D curve fit is based on SPARTICUS (2D-S and CPI) data and the SCPP field data have been grouped into size-bins; shown are the standard deviations (σ) in m and D for each size-bin. Mean values for m and D are shown by the intersection of the σ -bars.

Title Page

Abstract

Introduction

Conclusions

References

Tables

Figures

◀

▶

◀

▶

Back

Close

Full Screen / Esc

Printer-friendly Version

Interactive Discussion



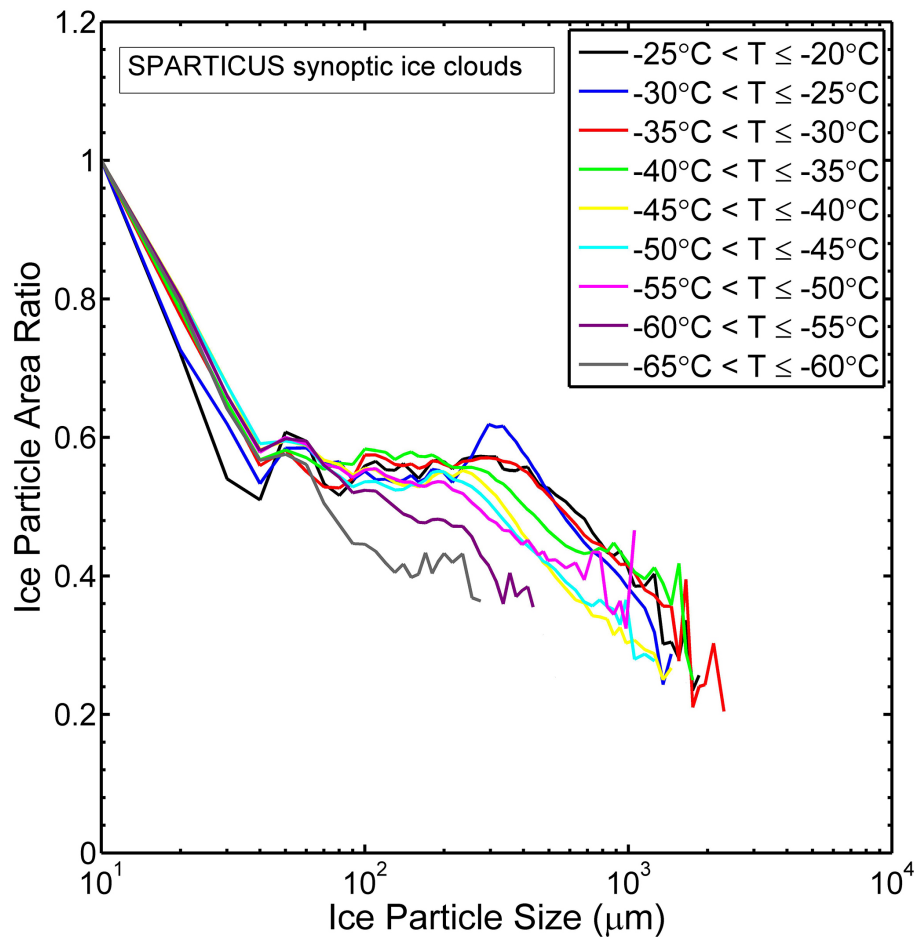


Figure 10. Mean area ratios for each mean PSD size-bin are shown as a proxy for ice particle shape. Temperature intervals corresponding to each mean PSD are indicated for synoptic ice clouds.

Ice particle mass- and area-dimension expressions

E. Erfani and
D. L. Mitchell

Title Page

Abstract Introduction

Conclusions References

Tables Figures

◀ ▶

◀ ▶

Back Close

Full Screen / Esc

Printer-friendly Version

Interactive Discussion



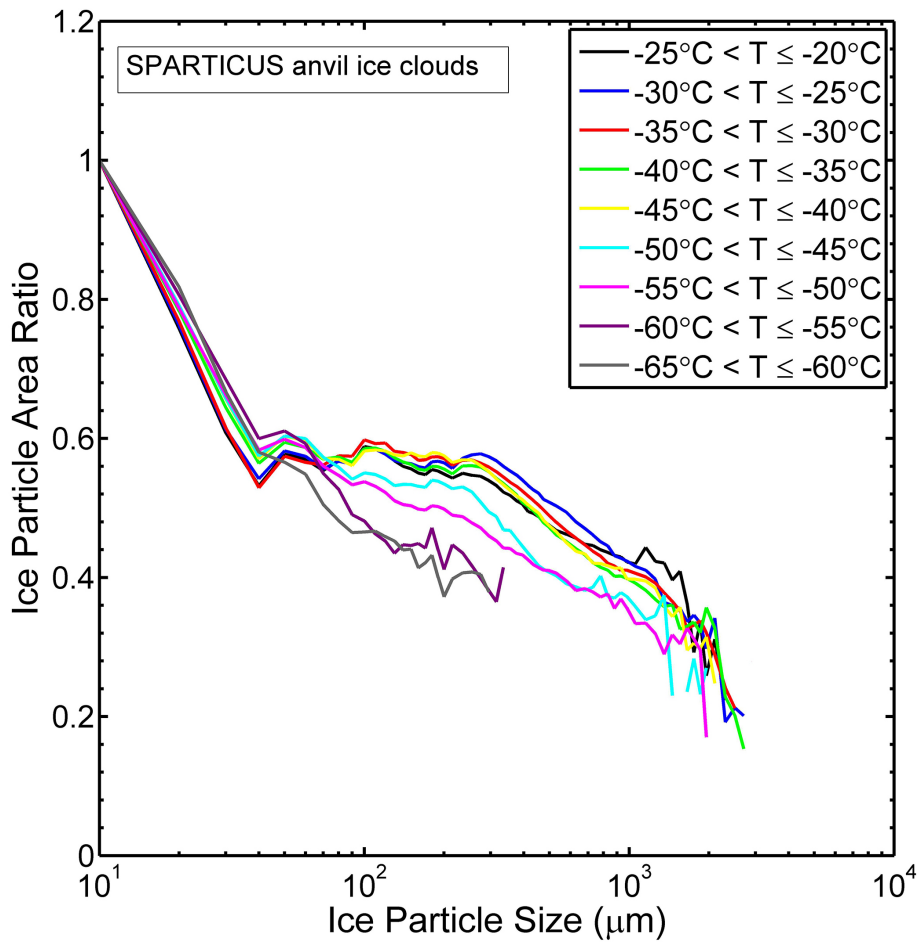


Figure 11. Same as Fig. 10, but for anvil ice clouds.

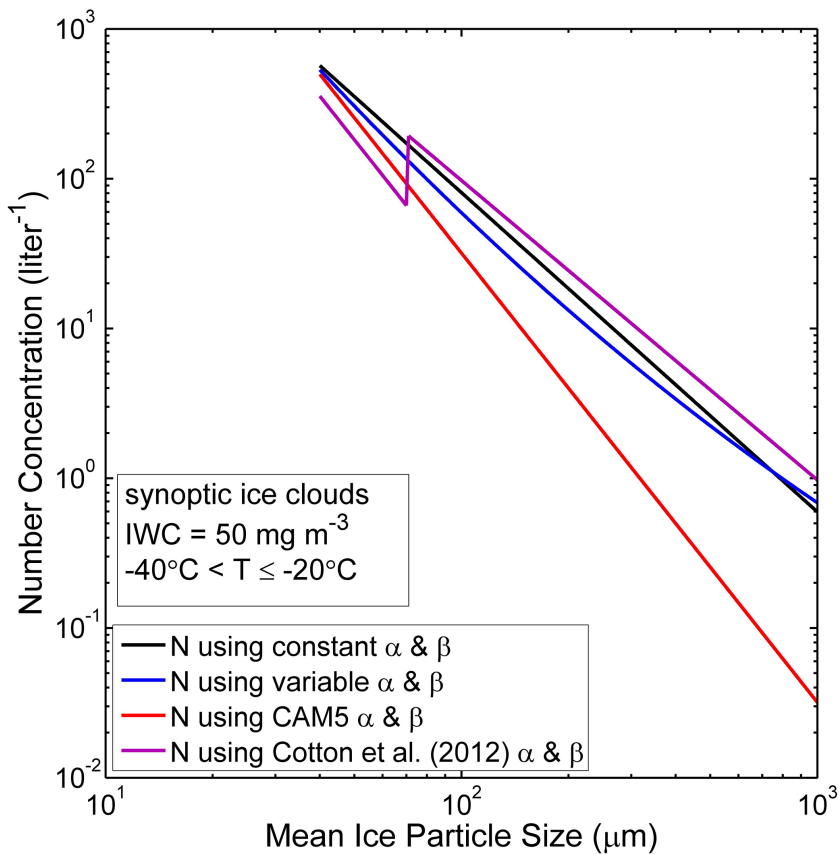


Figure 12. Dependence of the ice particle N on \bar{D} using the 4 methods indicated for determining α and β . The black and blue curves use the m - D curve fit based on Table 1 for the indicated temperature range, with the black curve α and β evaluated at $D = 500 \mu\text{m}$.

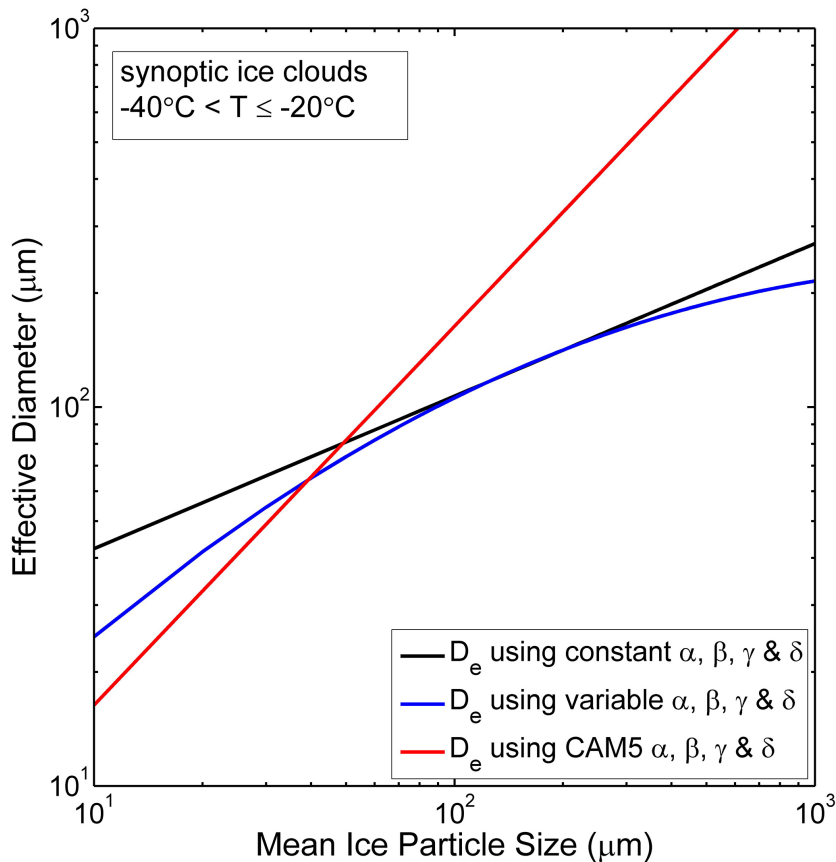


Figure 13. Dependence of the D_e on \bar{D} using the 3 methods indicated for determining α , β , γ and δ . The black and blue curves use the m - D curve fit based on Table 1 and A - D curve fit based on Table 2 for the indicated temperature range, with the black curve α , β , γ and δ evaluated at $D = 500 \mu\text{m}$.

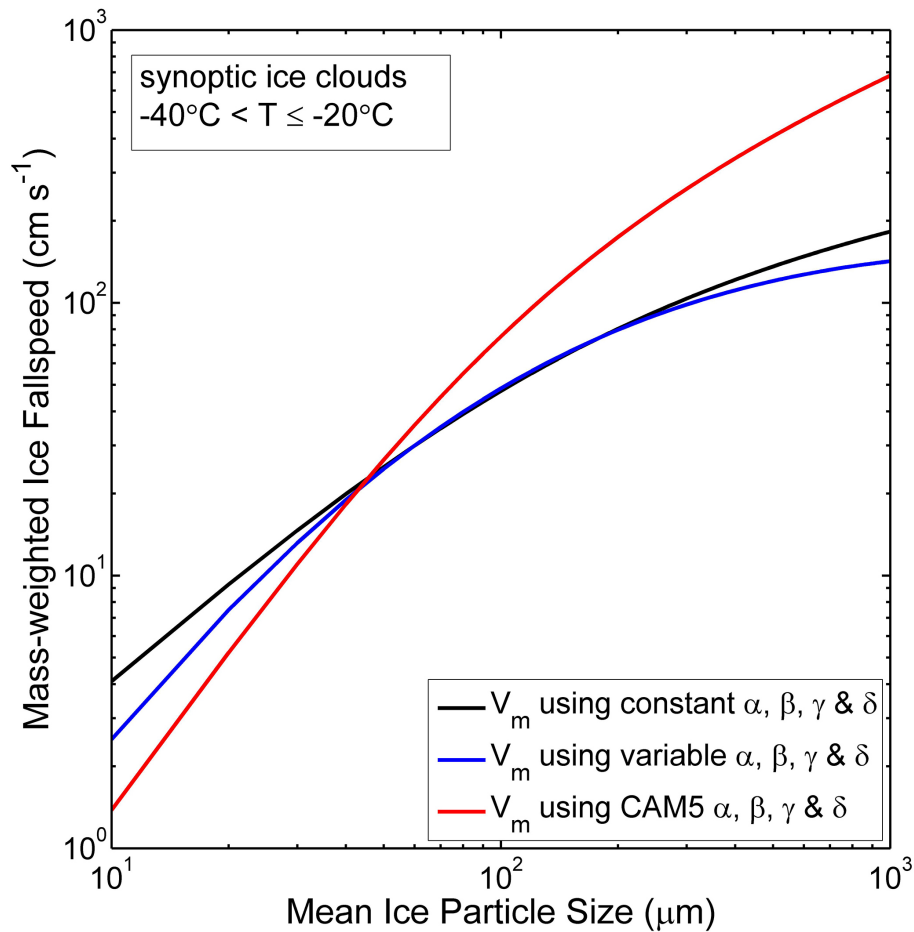


Figure 14. Same as Fig. 13, but for the dependence of V_m on \bar{D} .

Ice particle mass- and area-dimension expressions

E. Erfani and
D. L. Mitchell

Title Page

Abstract Introduction

Conclusions References

Tables Figures

◀ ▶

◀ ▶

Back Close

Full Screen / Esc

Printer-friendly Version

Interactive Discussion



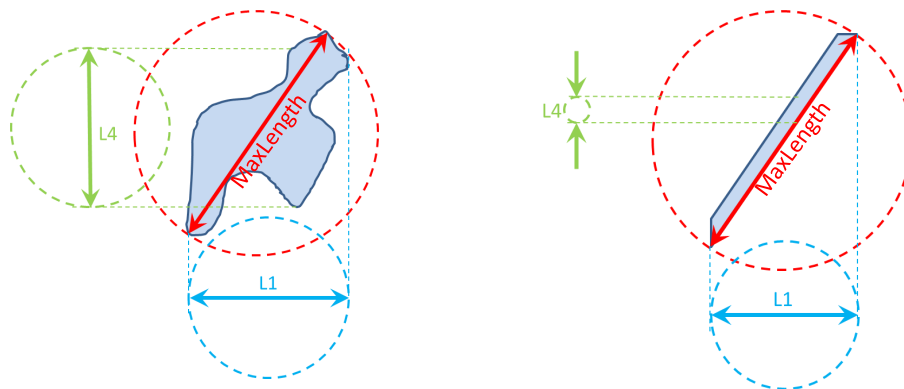


Figure A1. Geometry of dimension measurements showing length scales for the M1 method ($L1$) and the M7 method (Max.Length) for two different ice particle shapes. Courtesy of Paul Lawson and Sara Lance.

**Ice particle mass-
and area-dimension
expressions**

E. Erfani and
D. L. Mitchell

Title Page	
Abstract	Introduction
Conclusions	References
Tables	Figures
◀	▶
◀	▶
Back	Close
Full Screen / Esc	
Printer-friendly Version	
Interactive Discussion	



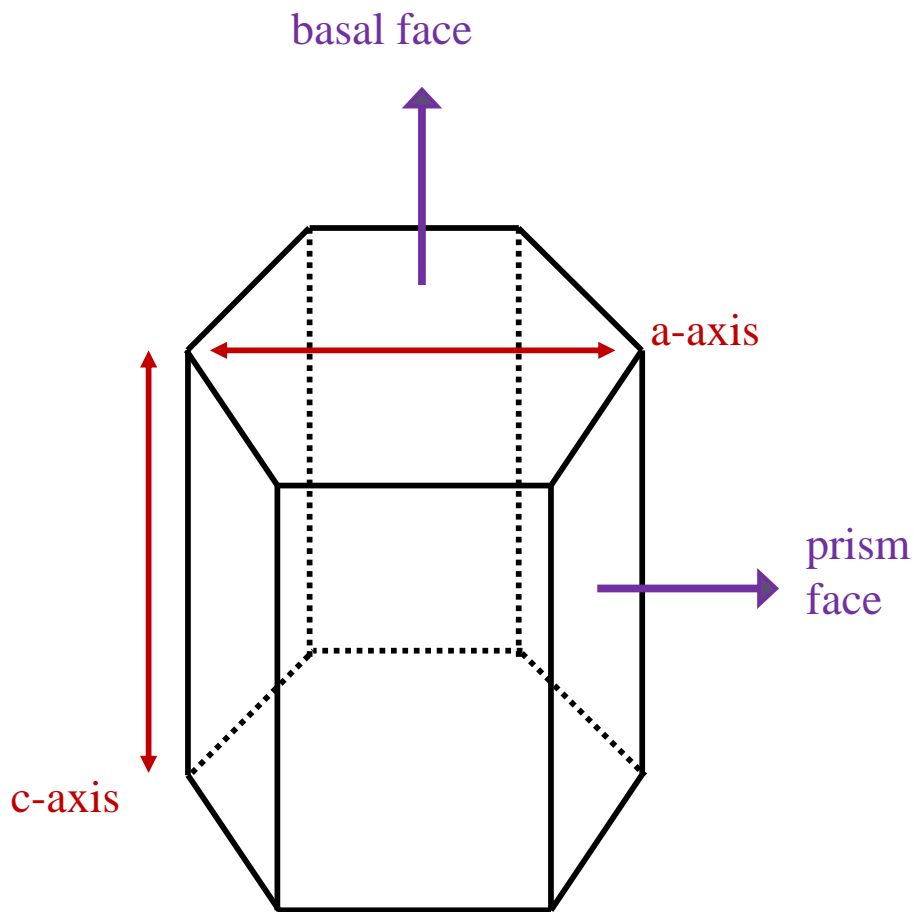


Figure B1. Geometry of hexagonal prism, representative of small ice crystals. See text for the definition of various symbols.

Ice particle mass-
and area-dimension
expressions

E. Erfani and
D. L. Mitchell

Title Page

Abstract

Introduction

Conclusions

References

Tables

Figures

◀

▶

◀

▶

Back

Close

Full Screen / Esc

Printer-friendly Version

Interactive Discussion

